

hep-ph/06xxx

Reexamining charmless $B \rightarrow PV$ decays in QCD factorization approach

Xinqiang Li^{1,2,3} and Yadong Yang¹ *

¹Department of Physics, Henan Normal University, Xinxiang, Henan 453007, P. R. China

²Institute of Theoretical Physics, Chinese Academy of Sciences, Beijing, 100080, P. R. China

³Graduate School of the Chinese Academy of Science, Beijing, 100039, P. R. China

December 2, 2024

Abstract

Using the QCD factorization approach, we reexamine the two-body hadronic charmless B -meson decays to final states involving a pseudoscalar (P) and a vector (V) meson, with inclusion of the important penguin contractions of the spectator-scattering amplitudes induced by the $b \rightarrow Dg^*g^*$ (with $D = d$ or s , and g^* denoting an off-shell gluon) transition, which are of order α_s^2 . Their impacts on the CP -averaged branching ratios and CP -violating asymmetries are also examined. We find that these higher order penguin contraction contributions have significant impacts on some specific decay modes. Since $B \rightarrow \pi K^*$, $K\rho$ decays involve the same electro-weak physics as $B \rightarrow \pi K$ puzzle, we present a detailed analysis for these decays and find that the five R-ratios for $B \rightarrow \pi K^*$, $K\rho$ system are in agreement with experimental data except $R(\pi K^*)$. Generally, these new contributions are found to be important for penguin-dominated $B \rightarrow PV$ decays.

PACS Numbers: 13.25Hw, 12.15Mm, 12.38Bx

*Corresponding author. E-mail address: yangyd@henannu.edu.cn

1 Introduction

The study of hadronic charmless B -meson decays can provide not only an interesting avenue to understand the CP violation and the flavor mixing of quark sector in the Standard Model (SM), but also powerful means to probe different new physics scenarios beyond the SM. With the operation of B -factory experiments, huge amount of experimental data on hadronic B -meson decays has been analyzed with appreciative precision. To account for these experimental data, theorists are urged to gain deep insight into the rare hadronic B -meson decays, and to reduce the theoretical uncertainties in determining the flavor parameters of the SM from experimental measurements.

In the past few years, much progress has been made in understanding the hadronic charmless B -meson decays: several novel methods have been proposed, such as the “naive” factorization (NF) [1], the perturbative QCD method (PQCD) [2], the QCD factorization (QCDF) [3, 4], the soft collinear effective theory (SCET) [5], and so on; Some model-independent methods based on (approximate) flavor symmetries have also been used to analysis the rare hadronic B -meson decays [6, 7, 8]. These methods usually have very different understandings of the B -meson decays, and hence the corresponding predictions are also quite different. The general comparison between these methods can be found, for example, in Ref. [9]. Since we shall adopt the QCDF approach in this paper, we would only focus on this approach below.

The QCD factorization approach, put forward by Beneke *et al.* a few years ago, has been widely used for analyzing the rare hadronic two-body B -meson decays [3, 10, 11, 12, 13, 14, 15, 16, 17, 18, 19, 20, 21]. The essence of this approach can be summarized as follows: since the b quark mass is much larger than the strong interaction scale Λ_{QCD} , in the heavy quark limit, the hadronic matrix elements relevant to the two-body hadronic B -meson decays can be represented in the following factorization form [3]

$$\begin{aligned} \langle M_1(p_1) M_2(p_2) | Q_i | B(p) \rangle &= \langle M_1(p_1) | j_1 | B(p) \rangle \langle M_2(p_2) | j_2 | 0 \rangle \\ &\times \left[1 + \sum r_n \alpha_s^n + \mathcal{O}(\Lambda_{\text{QCD}}/m_b) \right], \end{aligned} \quad (1)$$

where Q_i is the local four-quark operator in the effective weak Hamiltonian, $j_{1,2}$ are bilinear quark currents, and M_1 is the meson picking up the spectator quark from the B meson, while M_2 is the one which can be factored out from the (B, M_1) system. This scheme has incor-

porated elements of the NF approach (as the leading contribution) and the hard-scattering approach (as the sub-leading corrections). It provides a powerful means to compute systematically radiative (sub-leading nonfactorizable) corrections to the NF result for the hadronic matrix elements relevant to the two-body hadronic B -meson decays. In particular, the final-state strong interaction phases, which are very important for studying CP violation in B -meson decays, are calculable from first principles with this formalism. Detailed proofs and arguments related to this approach can be found in Refs. [3, 4]. Current status and recent developments of this approach have been reviewed recently in [22].

In a recent work [21], we have studied the higher order penguin contractions of the spectator-scattering amplitudes induced by $b \rightarrow Dg^*g^*$ transitions (where $D = d$ or s , depends on the specific decay modes, and the off-shell gluons g^* are either emitted from the internal quark loops, external quark lines, or splitted off the virtual gluon of the penguin diagrams), and investigated their impacts on the CP -averaged branching ratios and CP -violating asymmetries of $B \rightarrow \pi\pi, \pi K$ decays. We have found that these higher order corrections are not negligible in the exclusive two-body hadronic B -meson decays, in particular, in penguin-dominated $B \rightarrow \pi K$ decays. Thus, combining the findings in the literature [23, 24, 25, 26, 27, 28, 29], it should be very worthing to take account of these higher order penguin contraction contributions to both the inclusive and the exclusive B -meson decays. This encourages us to further investigate these effects on the hadronic charmless $B \rightarrow PV$ (where P and V denote pseudoscalar and vector mesons, respectively) decays.

Although the PV decay modes are closely related to their PP counterparts because of their similar flavor structures, they do have some advantages in some cases. For examples, due to the less penguin pollution, $B \rightarrow \pi\rho$ decays are more suitable than $B \rightarrow \pi\pi$ decays for extracting the weak angle α of the unitarity triangle of the Cabibbo-Kobayashi-Maskawa (CKM) quark-mixing matrix [30]. Studies on the two-body hadronic $B \rightarrow PV$ decays are therefore very helpful to deep our understandings of the rare hadronic B -meson decays. Earlier theoretical studies of $B \rightarrow PV$ decays based on various approaches can be found in Refs. [31, 32, 33, 34]. With the accumulation of new experimental data and the theoretical improvement, these $B \rightarrow PV$ decay modes have also been reanalyzed carefully [8, 12, 16, 19, 35]. In this paper, we will reexamine the hadronic charmless $B \rightarrow PV$ decays within the framework of the QCDF, taking account

of the higher order penguin contractions of the spectator-scattering amplitudes as mentioned above. Here we do not consider those decay modes with an η or η' meson in the final states, since in this case we will encounter many additional unknown parameters such as the contents, the mixing angles, and the anomaly $g - g - \eta^{(\prime)}$ coupling pertaining to these two particles, which have hindered us from getting reliable theoretical predictions.

This paper is organized as follows. Sec. 2 is devoted to the theoretical framework. In this section, we first give the relevant formulas describing the decay amplitudes for the hadronic charmless $B \rightarrow PV$ decays within the QCDF formalism at next-to-leading order in α_s , and then take into account the higher order penguin contraction contributions induced by the $b \rightarrow Dg^*g^*$ transition. In Sec. 3, we give our numerical results for the CP -averaged branching ratios and the CP -violating asymmetries of the hadronic charmless $B \rightarrow PV$ decays, and discuss the higher order penguin contraction contributions to these quantities. In addition, detailed analysis of the interesting decay modes, $B \rightarrow \pi K^*$ and $B \rightarrow K\rho$ decays, are also presented in this section. Finally, we conclude with a summary in Sec. 4. Some useful functions and the input parameters used in this paper are presented in Appendix A, B, respectively.

2 Theoretical framework for $B \rightarrow PV$ decays

2.1 The effective Hamiltonian for hadronic B -meson decays

Using the operator product expansion (OPE) and the renormalization group equation (RGE), the low energy effective Hamiltonian of the SM relevant to hadronic B -meson decays can be written as [36, 37]

$$\mathcal{H}_{\text{eff}} = \frac{G_F}{\sqrt{2}} \sum_{p=u,c} \lambda_p^{(\prime)} \left(C_1 Q_1^p + C_2 Q_2^p + \sum_{i=3,\dots,10} C_i Q_i + C_{7\gamma} Q_{7\gamma} + C_{8g} Q_{8g} \right) + \text{h.c.}, \quad (2)$$

where $\lambda_p = V_{pb} V_{ps}^*$ (for $b \rightarrow s$ transition) and $\lambda'_p = V_{pb} V_{pd}^*$ (for $b \rightarrow d$ transition) are products of the CKM matrix elements. The effective operators, Q_i , which govern a given decay process, can be expressed explicitly as follows.

(i) Current-current operators:

$$Q_1^p = (\bar{p}b)_{V-A} (\bar{D}p)_{V-A}, \quad Q_2^p = (\bar{p}_i b_j)_{V-A} (\bar{D}_j p_i)_{V-A}, \quad (3)$$

(ii) QCD-penguin operators:

$$\begin{aligned} Q_3 &= (\bar{D}b)_{V-A} \sum_q (\bar{q}q)_{V-A}, & Q_4 &= (\bar{D}_i b_j)_{V-A} \sum_q (\bar{q}_j q_i)_{V-A}, \\ Q_5 &= (\bar{D}b)_{V-A} \sum_q (\bar{q}q)_{V+A}, & Q_6 &= (\bar{D}_i b_j)_{V-A} \sum_q (\bar{q}_j q_i)_{V+A}, \end{aligned} \quad (4)$$

(iii) Electroweak penguin operators:

$$\begin{aligned} Q_7 &= (\bar{D}b)_{V-A} \sum_q \frac{3}{2} e_q (\bar{q}q)_{V+A}, & Q_8 &= (\bar{D}_i b_j)_{V-A} \sum_q \frac{3}{2} e_q (\bar{q}_j q_i)_{V+A}, \\ Q_9 &= (\bar{D}b)_{V-A} \sum_q \frac{3}{2} e_q (\bar{q}q)_{V-A}, & Q_{10} &= (\bar{D}_i b_j)_{V-A} \sum_q \frac{3}{2} e_q (\bar{q}_j q_i)_{V-A}, \end{aligned} \quad (5)$$

(iv) Electro- and chromo-magnetic dipole operators:

$$Q_{7\gamma} = -\frac{e}{8\pi^2} m_b \bar{D} \sigma_{\mu\nu} (1 + \gamma_5) F^{\mu\nu} b, \quad Q_{8g} = -\frac{g_s}{8\pi^2} m_b \bar{D} \sigma_{\mu\nu} (1 + \gamma_5) G^{\mu\nu} b, \quad (6)$$

where $(\bar{q}_1 q_2)_{V\pm A} = \bar{q}_1 \gamma_\mu (1 \pm \gamma_5) q_2$, i, j are colour indices, e_q are the electric charges of the quarks in units of $|e|$, and q denotes all the active quarks at scale $\mu = \mathcal{O}(m_b)$, i.e., $q' = u, d, s, c, b$. For decay modes induced by the $b \rightarrow d$ transition, $D = d$, while for the $b \rightarrow s$ transition induced ones, $D = s$.

The Wilson coefficients $C_i(\mu)$ in Eq. (2) represent all the contributions from physics with scale higher than $\mu \sim \mathcal{O}(m_b)$. They are first calculated at a high scale $\mu \sim M_W$ and then evolved down to a characteristic scale $\mu \sim m_b$ using RGE to the next-to-leading order. Numerical results for these coefficients evaluated at different scales can be found in Ref. [36].

2.2 Decay amplitudes at next-to-leading order in α_s

With the effective Hamiltonian given by Eq. (2), the decay amplitudes for a general hadronic charmless $B \rightarrow PV$ decay can be written as

$$\langle PV | \mathcal{H}_{\text{eff}} | B \rangle = \frac{G_F}{\sqrt{2}} \sum_{p=u,c} \lambda_p^{(\prime)} C_i \langle PV | Q_i^p | B \rangle. \quad (7)$$

Then, the most essential theoretical problem in describing the hadronic B -meson decays resides in the evaluation of the hadronic matrix element of the local operators $\langle PV | Q_i^p | B \rangle$. Within the formalism of the QCDF, this quantity could be greatly simplified. To leading power in

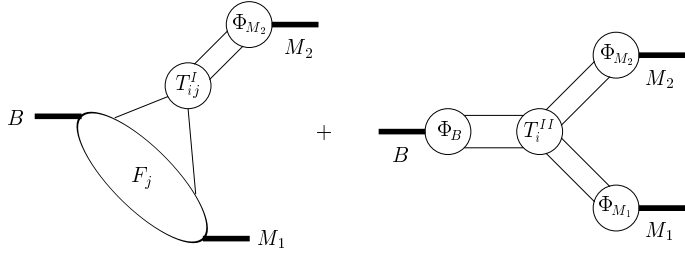


Figure 1: Graphical representation of the factorization formula. Only one of the two form-factor terms in Eq. (8) is shown for simplicity.

Λ_{QCD}/m_b , but to all orders in perturbation theory, it obeys the following factorization formula

$$\begin{aligned} \langle PV|Q_i^p|B\rangle &= F_1^{B \rightarrow P}(m_V^2) T_{V,i}^I * \Phi_V + A_0^{B \rightarrow V}(m_P^2) T_{P,i}^I * \Phi_P \\ &\quad + T_i^{II} * \Phi_B * \Phi_P * \Phi_V, \end{aligned} \quad (8)$$

where $F_1^{B \rightarrow P}$ and $A_0^{B \rightarrow V}$ denote the heavy-to-light $B \rightarrow P$ and $B \rightarrow V$ transition form factors, respectively. Φ_B , Φ_V , and Φ_P are the leading-twist light-cone distribution amplitudes (LCDAs) of valence quark Fock states for B , V , and P mesons, respectively. The $*$ products indicate an integration over the light-cone momentum fractions of the valence quarks inside the mesons. A graphical representation of this formula is shown in Fig. 1.

In the factorization formula given by Eq. (8), $T_i^{I,II}$ denote the hard-scattering kernels, which are dominated by hard gluon exchanges when the power suppressed $\mathcal{O}(\Lambda_{\text{QCD}}/m_b)$ terms are neglected. Thus, they are calculable order by order in perturbation theory. The relevant Feynman diagrams contributing to these kernels at next-to-leading in α_s are shown in Fig. 2. The leading terms of T_i^I come from the tree level diagrams, and the order of α_s terms of T_i^I can be depicted by the vertex-correction diagrams Fig. 2(a-d) and the penguin-correction diagrams Fig. 2(e-f). The kernel T_i^{II} describes the hard interactions between the spectator quark and the emitted meson M_2 where the gluon virtuality is also large. Its lowest order terms are of order α_s and can be depicted by the hard spectator-scattering diagrams Fig. 2(g-h). At the leading order in α_s , $T_i^I = 1$, $T_i^{II} = 0$, and the QCDF formula reproduce the NF results. As for the nonperturbative part, it is either power suppressed in Λ_{QCD}/m_b or can be separated into the transition form factors and the LCDAs of mesons.

With the above discussions on the effective Hamiltonian of hadronic B -meson decays and the QCDF formula of the hadronic matrix element, the decay amplitude of a general hadronic

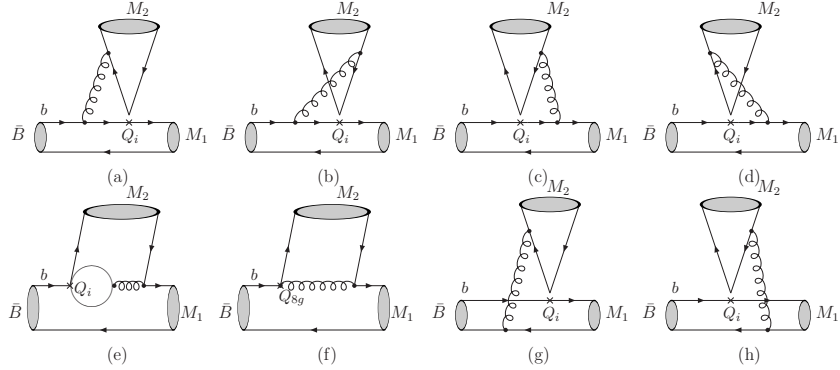


Figure 2: Order α_s corrections to the hard-scattering kernels $T_{M2,i}^I$ (coming from the diagrams (a)-(f)) and T_i^II (coming from the last two diagrams).

charmless $B \rightarrow PV$ decay, in the heavy quark limit, can then be written as

$$\mathcal{A}(B \rightarrow PV) = \frac{G_F}{\sqrt{2}} \sum_{p=u,c} \sum_{i=1}^{10} \lambda_p^{(i)} a_i^p \langle PV | Q_i | B \rangle_F, \quad (9)$$

where $\langle PV | Q_i | B \rangle_F$ is the factorized hadronic matrix element, which has the same definitions as that in the NF approach. The explicit expressions of the decay amplitudes for the hadronic charmless $B \rightarrow PV$ decays can be found, for example, in the Appendixes of Refs. [19, 31, 32]. All the “nonfactorizable” effects are encoded in the coefficients a_i^p , which are process dependent and can be calculated perturbatively. Following Beneke *et al.* [19], the general forms of the coefficients a_i^p ($i = 1$ to 10) at next-to-leading order in α_s , with M_1 being the meson picking up the spectator quark, can be written as

$$\begin{aligned} a_i^p(M_1 M_2) &= (C_i + \frac{C_{i\pm 1}}{N_c}) N_i(M_2) \\ &+ \frac{C_{i\pm 1}}{N_c} \frac{C_F \alpha_s}{4\pi} \left[V_i(M_2) + \frac{4\pi^2}{N_c} H_i(M_1 M_2) \right] + P_i^p(M_2), \end{aligned} \quad (10)$$

where the upper (lower) signs apply when i is odd (even). The quantities $V_i(M_2)$ account for one-loop vertex corrections, $H_i(M_1 M_2)$ for hard spectator interactions, and $P_i^p(M_2)$ for penguin contributions. The explicit expressions for these functions can be found in Ref. [19].

It is noted that, when calculating the decay amplitudes of hadronic charmless $B \rightarrow PV$ decays, the coefficients a_i^p ($i=3$ to 10) always appear in pairs. So one can define the following quantities α_i^p in terms of the coefficients a_i^p [19]

$$\alpha_1(M_1 M_2) = a_1(M_1 M_2),$$

$$\begin{aligned}
\alpha_2(M_1 M_2) &= a_2(M_1 M_2), \\
\alpha_3^p(M_1 M_2) &= \begin{cases} a_3^p(M_1 M_2) - a_5^p(M_1 M_2); & \text{if } M_1 M_2 = VP, \\ a_3^p(M_1 M_2) + a_5^p(M_1 M_2); & \text{if } M_1 M_2 = PV, \end{cases} \\
\alpha_4^p(M_1 M_2) &= \begin{cases} a_4^p(M_1 M_2) + r_\chi^{M_2} a_6^p(M_1 M_2); & \text{if } M_1 M_2 = PV, \\ a_4^p(M_1 M_2) - r_\chi^{M_2} a_6^p(M_1 M_2); & \text{if } M_1 M_2 = VP, \end{cases} \\
\alpha_{3,ew}^p(M_1 M_2) &= \begin{cases} a_9^p(M_1 M_2) - a_7^p(M_1 M_2); & \text{if } M_1 M_2 = VP, \\ a_9^p(M_1 M_2) + a_7^p(M_1 M_2); & \text{if } M_1 M_2 = PV, \end{cases} \\
\alpha_{4,ew}^p(M_1 M_2) &= \begin{cases} a_{10}^p(M_1 M_2) + r_\chi^{M_2} a_8^p(M_1 M_2); & \text{if } M_1 M_2 = PV, \\ a_{10}^p(M_1 M_2) - r_\chi^{M_2} a_8^p(M_1 M_2); & \text{if } M_1 M_2 = VP, \end{cases}
\end{aligned} \tag{11}$$

with M_1 being the meson that absorbs the spectator quark and M_2 the emitted meson. The scale-dependent ratio $r_\chi^{M_2}$ is defined as

$$r_\chi^P(\mu) = \frac{2 m_P^2}{m_b(\mu)(m_{q_1} + m_{q_2})(\mu)}, \quad r_\chi^V(\mu) = \frac{2 m_V}{m_b(\mu)} \frac{f_V^\perp(\mu)}{f_V}. \tag{12}$$

where all quark masses are the running current masses defined in the $\overline{\text{MS}}$ scheme, and $f_V^\perp(\mu)$ is the scale-dependent transverse decay constant of the vector meson. Although all these terms proportional to $r_\chi^{M_2}$ are formally power suppressed by Λ_{QCD}/m_b in the heavy-quark limit, they are chirally enhanced and numerically not small. Therefore, phenomenological applications of the QCDF method in hadronic B -meson decays requires at least a consistent inclusion of these chirally enhanced corrections.

According to the arguments in [3], the weak annihilation contributions to the decay amplitudes are power suppressed, and hence do not appear in the QCDF formula, Eq.(8). Nevertheless, as emphasized in Refs. [2, 38, 39], these contributions may be numerically important for realistic B -meson decays. In particular, the annihilation contributions with QCD corrections could give potentially large strong phases, hence large CP violation could be expected [2, 38]. It is therefore necessary to take the annihilation contributions into account. At leading order in α_s , the annihilation kernels arise from the four diagrams shown in Fig. 3. They result in a further contribution to the hard scattering kernel T_i^{II} in the QCDF formula, Eq.(8). However, within the formalism of QCDF, these annihilation topologies violate factorization because of the end-point divergence. In this work, following the treatment of Refs. [10, 40], we will introduce a cutoff to parameterize these contributions, and express the weak annihilation decay

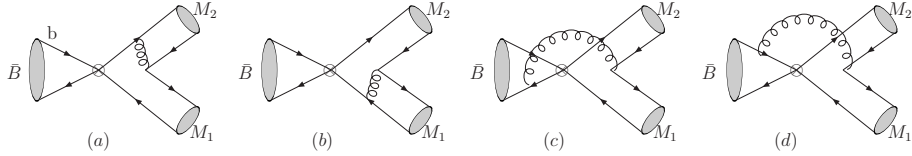


Figure 3: The weak annihilation diagrams of order α_s .

amplitudes as

$$\mathcal{A}^{ann}(B \rightarrow PV) \propto \frac{G_F}{\sqrt{2}} \sum_{p=u,c} \sum_i \lambda_p^{(i)} f_B f_{M_1} f_{M_2} b_i(M_1 M_2) \quad (13)$$

where f_B and f_M are the decay constants of the initial B and the final-state mesons, respectively. The parameters $b_i(M_1 M_2)$ describe the annihilation contributions, and their explicit expressions can be found in Refs. [10, 19]. The expressions of the weak annihilation decay amplitudes for hadronic charmless $B \rightarrow PV$ decays can be found in Refs. [16, 19].

It should be noted that, within the QCDF framework, all the “nonfactorizable” power suppressed contributions except for the hard spectator interactions and the weak annihilation contributions are neglected. In addition, in the evaluation of the hard spectator and the weak annihilation terms, the running coupling constant and the Wilson coefficients should be evaluated at an intermediate scale $\mu_h \sim (\Lambda_{\text{QCD}} m_b)^{1/2}$ rather than $\mu \sim m_b$. Specifically, we shall use $\mu_h = \sqrt{\Lambda_h \mu}$ with $\Lambda_h = 0.5$ GeV in our numerical calculations.

2.3 Penguin contractions of the spectator-scattering amplitudes of order α_s^2 and their contributions to $B \rightarrow PV$ decays

The recent global fit with the QCDF approach [17, 35, 41] indicate that the penguin amplitudes predicted with the QCDF approach are too small with too small strong phases relative to the tree amplitudes to account for the large branching ratios of some strange channels. As discussed in literature [23, 24, 25, 26, 27, 28, 42], the $b \rightarrow sgg$ transitions play an important role in the inclusive and semi-inclusive B -meson decays. In addition, in a recent work [21], we found that the higher order penguin contractions of the spectator-scattering amplitudes induced by the $b \rightarrow Dg^*g^*$ transition also play an important role in the exclusive two-body hadronic charmless B -meson decays. Motivated by these arguments, in this subsection, we shall investigate the higher order penguin contraction contributions to the hadronic charmless $B \rightarrow PV$ decays.

At the quark level, the $b \rightarrow Dg^*g^*$ transition can occur in many different manners as

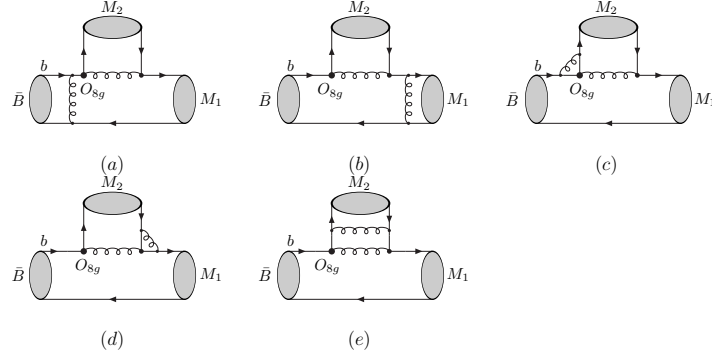


Figure 4: Representative diagrams induced by the $b \rightarrow Dg^*g^*$ transition which are not evaluated. Here we give only the chromo-magnetic dipole operator Q_{8g} contributions. With Q_{8g} replaced by the other operators, the corresponding diagrams for these operators can also be obtained.

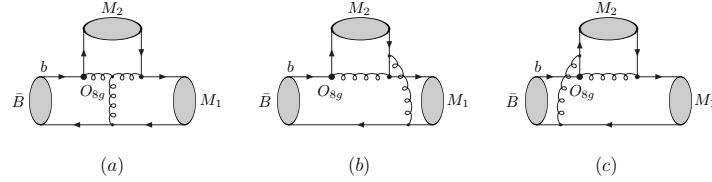


Figure 5: Chromo-magnetic operator Q_{8g} contributions induced by the $b \rightarrow Dg^*g^*$ transition.

depicted by Figs. 4–6. For example, one of the two gluons can radiate from the external quark line, while the other one coming from the chromo-magnetic dipole operator O_{8g} as Figs. 5(b) and 5(c) or from the internal quark loop in the penguin diagrams as Figs. 6(b) and 6(c). On the other hand, the two gluons can also radiate from the internal quark loop in Figs. 6(d) and 6(e) or split off the virtual gluon of the penguin diagrams as shown by Figs. 5(a) and 6(a). Here we do not consider the Feynman diagrams of the category shown in Fig. 4, since their contributions can be absorbed into the definition of the $B \rightarrow M_1$ transition form factors [Figs. 4(a) and 4(b)] and the LCDAs of the meson M_2 [Figs. 4(e)], or further suppressed by $\frac{g_s^2}{16\pi^2}$ [Figs. 4(c) and 4(d)]. It is easy to clarify this point by comparing the strengths of Fig. 4(c) to that of Fig. 5(a).

As shown by Figs. 5 and 6, these Feynman diagrams should be the dominant sources contributing to the penguin contractions of the spectator-scattering amplitudes of order α_s^2 , since they are not two-loop QCD diagrams, and hence there are no additional $\frac{1}{16\pi^2}$ suppression factor in their contributions compared to the genuine two-loop ones of order α_s^2 . Studies on these contributions could be very helpful for understanding the higher order perturbative corrections to

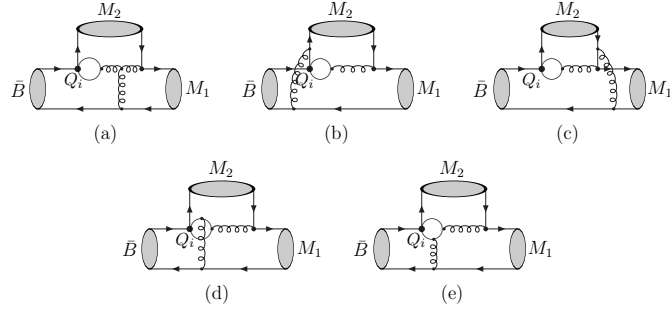


Figure 6: Penguin operator Q_i contributions induced by the $b \rightarrow Dg^*g^*$ transition.

the rare hadronic B -meson decays within the QCDF formalism. In the following, we shall evaluate these higher order penguin contractions of the spectator-scattering amplitudes induced by the $b \rightarrow Dg^*g^*$ transition, and discuss their contributions to the hadronic charmless $B \rightarrow PV$ decays.

We start with the calculation of the Feynman diagrams in Fig. 5. In this case, the b quark weak decay is induced by the chromo-magnetic dipole operator Q_{8g} . After direct calculation, we get

$$\begin{aligned} \mathcal{A}_{Q_{8g}} = & -i \frac{\alpha_s^2 f_B f_{M_1} f_{M_2}}{N_c^3} \lambda_t^{(\prime)} \int_0^1 d\xi \frac{\Phi_1^B(\xi)}{\xi} \\ & \times \int_0^1 du dv \left[\Phi_{M_2}(u) \Phi_{M_1}(v) + r_\chi^{M_1} r_\chi^{M_2} \Phi_{m_2}(u) \Phi_{m_1}(v) \right] \frac{8v - 27}{6(1-u)(1-v)v}, \end{aligned} \quad (14)$$

when M_1 is a pseudoscalar and M_2 a vector meson. For the opposite case of a vector M_1 and a pseudoscalar M_2 , one has to change the sign of the second term in the bracket of Eq. (14). Here $\lambda_t = V_{tb}V_{ts}^*$ (for the $b \rightarrow s$ transition) and $\lambda_t' = V_{tb}V_{td}^*$ (for the $b \rightarrow d$ transition) are products of the CKM matrix elements. As always, Φ_M and Φ_m denote the leading-twist and twist-3 LCDAs of the meson M in the final states, respectively.

In calculation of the Feynman diagrams of Fig. 6, we follow the method proposed by Greub and Liniger [26]. First, we calculate the fermion loops in these individual diagrams, and then insert these building blocks into the entire diagrams to obtain the total contributions. In evaluating the internal quark loop diagrams, we shall adopt the naive dimensional regularization (NDR) scheme and the modified minimal subtraction ($\overline{\text{MS}}$) scheme. In addition, we shall adopt the *ad hoc* Feynman gauge for the gluon propagator throughout this paper. Analogous to the calculation of the penguin diagrams in Fig. 2(e), we should also consider two distinct

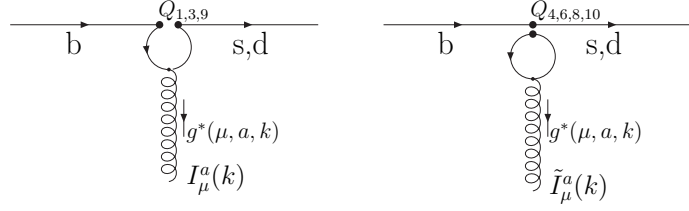


Figure 7: Building blocks $I_\mu^a(k)$ (associated with the contraction of the operators $Q_{1,3,9}$) and $\tilde{I}_\mu^a(k)$ (associated with the contraction of the operators $Q_{4,6,8,10}$) for Figs. 6(a)–6(c).

contractions in the weak interaction vertex of the penguin operators.

As can be seen from Fig. 6, the first three Feynman diagrams have the same building block $I_\mu^a(k)$ (corresponding to the contraction of operators $Q_{1,3,9}$) or $\tilde{I}_\mu^a(k)$ (corresponding to the contractions of the operators $Q_{4,6,8,10}$). These building blocks are depicted by Fig. 7 and given by

$$I_\mu^a(k) = \frac{g_s}{4\pi^2} \Gamma\left(\frac{\epsilon}{2}\right) (2-\epsilon) (4\pi\mu^2)^{\frac{\epsilon}{2}} (k_\mu \not{k} - k^2 \gamma_\mu) (1 - \gamma_5) T^a \times \int_0^1 dx \frac{x(1-x)}{\left[m_q^2 - x(1-x)k^2 - i\delta\right]^{\frac{\epsilon}{2}}}, \quad (15)$$

$$\tilde{I}_\mu^a(k) = \frac{g_s}{2\pi^2} \Gamma\left(\frac{\epsilon}{2}\right) (4\pi\mu^2)^{\frac{\epsilon}{2}} (k_\mu \not{k} - k^2 \gamma_\mu) (1 - \gamma_5) T^a \times \int_0^1 dx \frac{x(1-x)}{\left[m_q^2 - x(1-x)k^2 - i\delta\right]^{\frac{\epsilon}{2}}}, \quad (16)$$

where k is the momentum of gluon, $T^a = \frac{\lambda^a}{2}$, with λ^a the Gell-Mann matrices, g_s is the strong coupling constant, and m_q the pole mass of the quark propagating in the quark loop. The free indices μ and a should be contracted with the gluon propagator when inserting these building blocks into the entire Feynman diagrams. Here we have used $d = 4 - \epsilon$.

After performing the subtraction with the $\overline{\text{MS}}$ scheme, we get

$$I_\mu^a(k) = -\frac{g_s}{8\pi^2} \left[\frac{2}{3} - \frac{4}{3} \ln \frac{\mu}{m_b} - G(s_q, r) \right] (k_\mu \not{k} - k^2 \gamma_\mu) (1 - \gamma_5) T^a, \quad (17)$$

$$\tilde{I}_\mu^a(k) = -\frac{g_s}{8\pi^2} \left[-\frac{4}{3} \ln \frac{\mu}{m_b} - G(s_q, r) \right] (k_\mu \not{k} - k^2 \gamma_\mu) (1 - \gamma_5) T^a, \quad (18)$$

with the function $G(s, r)$ defined by

$$G(s, r) = -4 \int_0^1 dx x(1-x) \ln[s - x(1-x)r - i\delta], \quad (19)$$

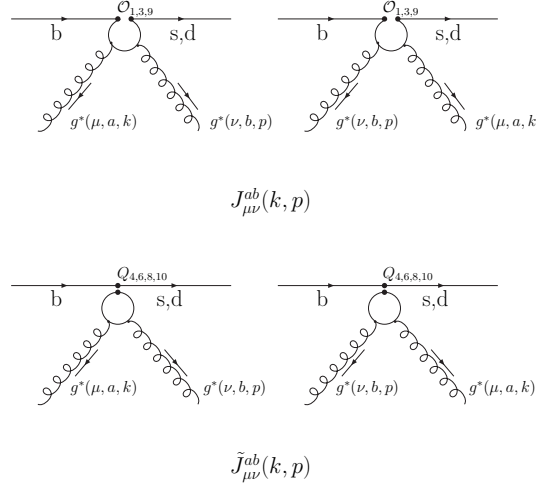


Figure 8: Building blocks $J_{\mu\nu}^{ab}(k, p)$ (associated with the contractions of the operators $Q_{1,3}$) and $\tilde{J}_{\mu\nu}^{ab}(k, p)$ (associated with the contractions of the operators $Q_{4,6}$) for Figs. 6(d) and 6(e).

where the term $i\delta$ is the “ ϵ -prescription”, and $r = k^2/m_b^2$.

The sum of the fermion loops in the last two diagrams in Fig. 6 are denoted by the building block $J_{\mu\nu}^{ab}(k, p)$ (corresponding to the contraction of operators $Q_{1,3,9}$) or $\tilde{J}_{\mu\nu}^{ab}(k, p)$ (corresponding to the contraction of operators $Q_{4,6,8,10}$), which are depicted by Fig. 8. Using the decomposition advocated by [25, 26], these building blocks can be expressed as

$$J_{\mu\nu}^{ab}(k, p) = T_{\mu\nu}^+(k, p) \{T^a, T^b\} + T_{\mu\nu}^-(k, p) [T^a, T^b], \quad (20)$$

$$\tilde{J}_{\mu\nu}^{ab}(k, p) = \tilde{T}_{\mu\nu}^+(k, p) \{T^a, T^b\} + \tilde{T}_{\mu\nu}^-(k, p) [T^a, T^b], \quad (21)$$

where the first part is symmetric, while the second one is antisymmetric with respect to the color structures of the two off-shell gluons. Here $k(p)$, $a(b)$, and $\mu(\nu)$ are the momentum, color, and polarization of the off-shell gluons. Below, we refer to the gluon with indices (ν, b, p) as the one connecting with the spectator quark.

In the NDR scheme, after integrating over the (shifted) loop momentum, we can represent the quantities $T_{\mu\nu}^\pm(k, p)$ and $\tilde{T}_{\mu\nu}^\pm(k, p)$ as [25, 26]

$$\begin{aligned} T_{\mu\nu}^+(k, p) = & \frac{\alpha_s}{4\pi} \left[E(\mu, \nu, k) \Delta i_5 + E(\mu, \nu, p) \Delta i_6 \right. \\ & - E(\mu, k, p) \frac{k_\nu}{k \cdot p} \Delta i_{23} - E(\mu, k, p) \frac{p_\nu}{k \cdot p} \Delta i_{24} \\ & \left. - E(\nu, k, p) \frac{k_\mu}{k \cdot p} \Delta i_{25} - E(\nu, k, p) \frac{p_\mu}{k \cdot p} \Delta i_{26} \right] (1 - \gamma_5), \end{aligned} \quad (22)$$

$$\begin{aligned}
T_{\mu\nu}^-(k, p) &= \frac{\alpha_s}{4\pi} \left[\not{k} g_{\mu\nu} \Delta i_2 + \not{p} g_{\mu\nu} \Delta i_3 \right. \\
&\quad + \gamma_\mu k_\nu \Delta i_8 + \gamma_\mu p_\nu \Delta i_9 + \gamma_\nu k_\mu \Delta i_{11} + \gamma_\nu p_\mu \Delta i_{12} \\
&\quad + \not{k} \frac{k_\mu k_\nu}{k \cdot p} \Delta i_{15} + \not{k} \frac{k_\mu p_\nu}{k \cdot p} \Delta i_{16} + \not{k} \frac{p_\mu k_\nu}{k \cdot p} \Delta i_{17} + \not{k} \frac{p_\mu p_\nu}{k \cdot p} \Delta i_{18} \\
&\quad \left. + \not{p} \frac{k_\mu k_\nu}{k \cdot p} \Delta i_{19} + \not{p} \frac{k_\mu p_\nu}{k \cdot p} \Delta i_{20} + \not{p} \frac{p_\mu k_\nu}{k \cdot p} \Delta i_{21} + \not{p} \frac{p_\mu p_\nu}{k \cdot p} \Delta i_{22} \right] (1 - \gamma_5), \quad (23)
\end{aligned}$$

$$\tilde{T}_{\mu\nu}^+(k, p) = a T_{\mu\nu}^+(k, p), \quad (24)$$

$$\begin{aligned}
\tilde{T}_{\mu\nu}^-(k, p) &= T_{\mu\nu}^-(k, p) + \frac{\alpha_s}{4\pi} \left[\not{k} g_{\mu\nu} \frac{4}{3} - \not{p} g_{\mu\nu} \frac{4}{3} - \gamma_\mu k_\nu \frac{8}{3} - \gamma_\mu p_\nu \frac{4}{3} \right. \\
&\quad \left. + \gamma_\nu k_\mu \frac{4}{3} + \gamma_\nu p_\mu \frac{8}{3} \right] (1 - \gamma_5), \quad (25)
\end{aligned}$$

where the matrix E in Eq. (22) is defined by

$$\begin{aligned}
E(\mu, \nu, k) &= \gamma_\mu \gamma_\nu \not{k} - \gamma_\mu k_\nu + \gamma_\nu k_\mu - \not{k} g_{\mu\nu} \\
&= -i \epsilon_{\mu\nu\alpha\beta} k^\alpha \gamma^\beta \gamma_5, \quad (26)
\end{aligned}$$

with the second line obtained in a four dimension context with the Bjorken-Drell conventions. The parameter a in Eq. (25) denotes the chiral structure of the local four-quark operators in the weak interaction vertex with $a = \pm$ corresponding to $(V - A) \otimes (V \mp A)$, respectively. The explicit forms of the dimensionally regularized expressions for the Δi functions can be found in Appendix B of Ref. [21].

Equipped with the explicit forms of these building blocks, we can now evaluate all the Feynman diagrams in Fig. 6. After direct calculations, the final results for these penguin contractions of spectator-scattering amplitudes for hadronic charmless $B \rightarrow PV$ decay modes, with the subscript denoting the contraction of the corresponding operator in the weak interaction vertex, can be expressed as

$$\begin{aligned}
\mathcal{A}_{Q_1} &= i \frac{\alpha_s^2 f_B f_{M_1} f_{M_2}}{N_c^3} \lambda_p^{(\prime)} \int_0^1 d\xi \frac{\Phi_1^B(\xi)}{\xi} \int_0^1 du dv \left\{ \left[\frac{2}{3} - \frac{4}{3} \ln \frac{\mu}{m_b} - G(s_p, \bar{u}) \right] f_1(u, v) \right. \\
&\quad \left. + \left[\frac{2}{3} - \frac{4}{3} \ln \frac{\mu}{m_b} - G(s_p, \bar{u}v) \right] f_2(u, v) + f_1(u, v, m_p) \right\}, \quad (27)
\end{aligned}$$

$$\begin{aligned}
\mathcal{A}_{Q_3} &= -i \frac{\alpha_s^2 f_B f_{M_1} f_{M_2}}{N_c^3} \lambda_t^{(\prime)} \int_0^1 d\xi \frac{\Phi_1^B(\xi)}{\xi} \int_0^1 du dv \left\{ [f_1(u, v, 0) + f_1(u, v, 1)] \right. \\
&\quad + \left[\frac{4}{3} - \frac{8}{3} \ln \frac{\mu}{m_b} - G(0, \bar{u}) - G(1, \bar{u}) \right] f_1(u, v) \\
&\quad \left. + \left[\frac{4}{3} - \frac{8}{3} \ln \frac{\mu}{m_b} - G(0, \bar{u}v) - G(1, \bar{u}v) \right] f_2(u, v) \right\}, \quad (28)
\end{aligned}$$

$$\mathcal{A}_{Q_9} = -\frac{1}{2} \mathcal{A}_{Q_3}, \quad (29)$$

$$\begin{aligned} \mathcal{A}_{Q_4} = & -i \frac{\alpha_s^2 f_B f_{M_1} f_{M_2}}{N_c^3} \lambda_t^{(\prime)} \int_0^1 d\xi \frac{\Phi_1^B(\xi)}{\xi} \int_0^1 du dv \left\{ [(n_f - 2) f_2(u, v, 0) + f_2(u, v, m_c) \right. \\ & + f_2(u, v, m_b)] + \left[-\frac{4 n_f}{3} \ln \frac{\mu}{m_b} - (n_f - 2) G(0, \bar{u}) - G(s_c, \bar{u}) - G(1, \bar{u}) \right] f_1(u, v) \\ & + \left. \left[-\frac{4 n_f}{3} \ln \frac{\mu}{m_b} - (n_f - 2) G(0, \bar{u} v) - G(s_c, \bar{u} v) - G(1, \bar{u} v) \right] f_2(u, v) \right\}, \end{aligned} \quad (30)$$

$$\mathcal{A}_{Q_6} = \mathcal{A}_{Q_4}, \quad (31)$$

$$\begin{aligned} \mathcal{A}_{Q_8} = & -i \frac{\alpha_s^2 f_B f_{M_1} f_{M_2}}{N_c^3} \lambda_t^{(\prime)} \int_0^1 d\xi \frac{\Phi_1^B(\xi)}{\xi} \int_0^1 du dv \left\{ \left[f_2(u, v, m_c) - \frac{1}{2} f_2(u, v, m_b) \right] \right. \\ & + \left[-\frac{2}{3} \ln \frac{\mu}{m_b} - G(s_c, \bar{u}) + \frac{1}{2} G(1, \bar{u}) \right] f_1(u, v) \\ & + \left. \left[-\frac{2}{3} \ln \frac{\mu}{m_b} - G(s_c, \bar{u} v) + \frac{1}{2} G(1, \bar{u} v) \right] f_2(u, v) \right\}, \end{aligned} \quad (32)$$

$$\mathcal{A}_{Q_{10}} = \mathcal{A}_{Q_8}, \quad (33)$$

with

$$\begin{aligned} f_1(u, v) = & r_\chi^{M_2} \Phi_{m_2}(u) \Phi_{M_1}(v) \frac{(9 - 8v)(3 - v)}{12(1 - v)^2 v} \\ & + r_\chi^{M_1} \Phi_{M_2}(u) \Phi_{m_1}(v) \frac{27 - 8v}{12(1 - u)(1 - v)v}, \end{aligned} \quad (34)$$

$$f_2(u, v) = -r_\chi^{M_2} \Phi_{m_2}(u) \Phi_{M_1}(v) \frac{1}{6(1 - v)^2} + r_\chi^{M_1} \Phi_{M_2}(u) \Phi_{m_1}(v) \frac{1}{6u(1 - v)}, \quad (35)$$

$$\begin{aligned} f_1(u, v, m_q) = & r_\chi^{M_2} \Phi_{m_2}(u) \Phi_{M_1}(v) \frac{3}{8(1 - v)v} (\Delta i_2 - \Delta i_8) \\ & + r_\chi^{M_1} \Phi_{M_2}(u) \Phi_{m_1}(v) \left[\frac{3}{8(1 - u)(1 - v)v} (\Delta i_3 + 2\Delta i_{12} + \Delta i_{21}) \right. \\ & \left. + \frac{3}{8(1 - u)(1 - v)} (\Delta i_2 - \Delta i_3 - \Delta i_8 - 2\Delta i_{12} + \Delta i_{17} - \Delta i_{21}) \right], \end{aligned} \quad (36)$$

$$\begin{aligned} f_2(u, v, m_q) = & r_\chi^{M_2} \Phi_{m_2}(u) \Phi_{M_1}(v) \frac{3}{8(1 - v)v} (4 + \Delta i_2 - \Delta i_8) \\ & + r_\chi^{M_1} \Phi_{M_2}(u) \Phi_{m_1}(v) \left[\frac{3}{8(1 - u)(1 - v)v} (4 + \Delta i_3 + 2\Delta i_{12} + \Delta i_{21}) \right. \\ & \left. + \frac{3}{8(1 - u)(1 - v)} (\Delta i_2 - \Delta i_3 - \Delta i_8 - 2\Delta i_{12} + \Delta i_{17} - \Delta i_{21}) \right], \end{aligned} \quad (37)$$

when M_1 is a pseudoscalar and M_2 a vector meson. For the opposite case, i.e., M_1 is a vector and M_2 a pseudoscalar meson, one needs only change the sign of the first term in the functions f_i defined above. The argument m_q in the above functions f_i is the pole quark mass propagating in the fermion loops. At this stage, the Δ_i functions appearing in Eqs. (36) and 37 are the ones

that have been performed the Feynman parameter integrals, whose explicit forms can be found in Appendix B of Refs. [21, 28]. For convenience, we also list them in Appendix A.

With the individual operator contributions given above, the total contributions of the penguin contractions of spectator-scattering amplitudes to a general hadronic charmless $B \rightarrow PV$ decays can be written as

$$\begin{aligned} \mathcal{A}'(B \rightarrow PV) = & \frac{G_F}{\sqrt{2}} \left[\sum_{p=u,c} C_1 \mathcal{A}_{Q_1} + \left(C_3 - \frac{1}{2} C_9 \right) \mathcal{A}_{Q_3} + \left(C_4 + C_6 \right) \mathcal{A}_{Q_4} \right. \\ & \left. + \left(C_8 + C_{10} \right) \mathcal{A}_{Q_8} + C_{8g}^{\text{eff}} \mathcal{A}_{Q_{8g}} \right], \end{aligned} \quad (38)$$

where we have used the relations in Eqs. (29), (31), and (33), and the superscript ‘ \prime ’ of the decay amplitude indicate the one to be distinguished from the next-to-leading order results given by Eqs. (9) and (13). The total decay amplitudes for a general hadronic charmless $B \rightarrow PV$ decays are then the sum of these three pieces

$$\langle PV | \mathcal{H}_{\text{eff}} | B \rangle = \mathcal{A}(B \rightarrow PV) + \mathcal{A}^{\text{ann}}(B \rightarrow PV) + \mathcal{A}'(B \rightarrow PV), \quad (39)$$

where the first two pieces have already been taken into account [17, 19], while the last one, representing contributions of the penguin contractions of spectator-scattering amplitudes of order α_s^2 , has not been considered previously with the QCDF approach.

3 Numerical results and discussions

With the theoretical expressions and the input parameters as collected in Appendix B, we can now evaluate the branching ratios and the direct CP -violating asymmetries of the two-body hadronic charmless $B \rightarrow PV$ decays, with $P = (\pi, K)$ and $V = (\rho, \omega, K^*, \phi)$. For each quantity, we first give the predictions at next-to-leading order in α_s , and then take into account the higher order penguin contractions of spectator-scattering amplitudes induced by the $b \rightarrow Dg^*g^*$ transition. The combined contribution of these two pieces, denoted by $\mathcal{O}(\alpha_s + \alpha_s^2)$, is then given in the last. For comparison, results of the NF approximation are also presented. All the experimental data are taken from the home page of the Heavy Flavor Averaging Group (HFAG) [43].

3.1 Branching ratios of $B \rightarrow PV$ decays

With the total decay amplitudes given by Eq. (39), the branching ratios of a general hadronic charmless $B \rightarrow PV$ decays in the B -meson rest frame can be written as

$$\mathcal{B}(B \rightarrow PV) = \frac{\tau_B}{8\pi m_B^2} |P_c| |\langle PV | \mathcal{H}_{\text{eff}} | B \rangle|^2, \quad (40)$$

where τ_B is the lifetime of B meson, and $|P_c|$ is the absolute value of the momentum of final-state hadrons in the B -meson rest frame and given by

$$|P_c| = \frac{\sqrt{[m_B^2 - (m_P + m_V)^2][m_B^2 - (m_P - m_V)^2]}}{2m_B}. \quad (41)$$

The branching ratios of the CP -conjugated decay modes can be obtained from Eq.(40) by replacing the CKM factors with their complex conjugate in the expressions of the decay amplitudes. The CP -averaged branching ratio of a B -meson decays into a general final state f are then expressed as

$$\bar{\mathcal{B}}(B \rightarrow f) = \frac{1}{2} [\mathcal{B}(B \rightarrow f) + \mathcal{B}(\bar{B} \rightarrow \bar{f})]. \quad (42)$$

In the following discussions, we classify the charmless $B \rightarrow PV$ decays into two categories: the strange-changing ($\Delta S = 1$) and the strange-conserving ($\Delta S = 0$) processes. Considering the hierarchies of the CKM matrix elements and the magnitudes of the Wilson coefficients, we expect that the $\Delta S = 1$ decay channels are generally penguin-dominated, while the $\Delta S = 0$ ones are tree-dominated. In addition, the higher order penguin contractions of the spectator-scattering amplitudes are expected to have a bigger impact on the $\Delta S = 1$ processes than on the $\Delta S = 0$ processes, because of the CKM factor suppressions in the latter. Numerical results of the CP -averaged branching ratios for these hadronic charmless $B \rightarrow PV$ decays are collected in Tables 1 and 2, where $\bar{\mathcal{B}}^f$ and $\bar{\mathcal{B}}^{f+a}$ denote the results without and with the annihilation contributions, respectively. The NF results, which are of order $\mathcal{O}(\alpha_s^0)$, are also shown for comparison.

For penguin-dominated $\Delta S = 1$ decays, since the “nonfactorizable” effects have large contributions to the QCD penguin coefficients $\alpha_{3,4}^p$, the predicted branching ratios with the QCDF approach are usually quite different from those obtained with the NF approximation. In addition, the weak annihilation contributions to these decay channels are also quite sizable. Combining the numerical results given by Table 1, we have the following remarks.

Table 1: The CP -averaged branching ratios (in units of 10^{-6}) of the hadronic charmless $B \rightarrow PV$ decays with $\Delta S = 1$. $\bar{\mathcal{B}}^f$ and $\bar{\mathcal{B}}^{f+a}$ denote the results without and with the annihilation contributions, respectively. The NF results, which are of order $\mathcal{O}(\alpha_s^0)$, are also shown for comparison. $\bar{\rho} = 0.20$ and $\bar{\eta} = 0.33$.

Decay Modes	NF	$\bar{\mathcal{B}}^f$		$\bar{\mathcal{B}}^{f+a}$		Experiment
		$\mathcal{O}(\alpha_s)$	$\mathcal{O}(\alpha_s + \alpha_s^2)$	$\mathcal{O}(\alpha_s)$	$\mathcal{O}(\alpha_s + \alpha_s^2)$	
$B^- \rightarrow \pi^- \bar{K}^{*0}$	2.59	2.90	4.24	4.37	5.99	10.8 ± 0.8
$B^- \rightarrow \pi^0 K^{*-}$	1.97	2.06	2.77	2.82	3.66	6.9 ± 2.3
$\bar{B}^0 \rightarrow \pi^+ K^{*-}$	1.99	2.10	3.02	3.06	4.23	$11.7^{+1.5}_{-1.4}$
$\bar{B}^0 \rightarrow \pi^0 \bar{K}^{*0}$	0.54	0.61	1.04	1.06	1.62	1.7 ± 0.8
$B^- \rightarrow \bar{K}^0 \rho^-$	0.77	1.31	0.89	3.48	2.76	< 48
$B^- \rightarrow K^- \rho^0$	0.57	0.69	0.56	1.48	1.20	$4.23^{+0.56}_{-0.57}$
$\bar{B}^0 \rightarrow K^- \rho^+$	1.91	2.66	2.13	5.29	4.49	$9.9^{+1.6}_{-1.5}$
$\bar{B}^0 \rightarrow \bar{K}^0 \rho^0$	1.24	1.71	1.37	3.30	2.83	5.1 ± 1.6
$B^- \rightarrow K^- \omega$	0.64	1.62	1.34	2.95	2.53	6.5 ± 0.6
$\bar{B}^0 \rightarrow \bar{K}^0 \omega$	0.09	0.74	0.53	1.80	1.47	4.7 ± 0.6
$B^- \rightarrow K^- \phi$	4.16	3.25	5.09	5.36	7.67	$9.03^{+0.65}_{-0.63}$
$\bar{B}^0 \rightarrow \bar{K}^0 \phi$	3.82	2.99	4.68	4.84	6.95	$8.3^{+1.2}_{-1.0}$

- The decays $B \rightarrow \pi K^*$ and $B \rightarrow K\phi$. The predicted CP -averaged branching ratios of these decay modes are consistently lower than the experimental data. The dominant contributions to the decay amplitudes of these decay modes are proportional to the coefficient $\alpha_4^p(PV) = a_4^p(PV) + r_\chi^V a_6^p(PV)$. The weak annihilation contributions and the higher order penguin contraction contributions can give enhancements to these branching ratios by about $30\% \sim 70\%$. With the inclusion of these two effects, the discrepancy between the theoretical predictions and the experimental data can be reduced significantly. In addition, large interference effects between the tree and the penguin amplitudes in some decay channels, such as the decays $\bar{B}^0 \rightarrow \pi^+ K^{*-}$ and $B^- \rightarrow \pi^0 K^{*-}$, are expected. It is thus possible to extract the weak angle $\gamma = \arg(V_{ub}^*)$ from these decay channels, which

Table 2: The CP -averaged branching ratios (in units of 10^{-6}) of the hadronic charmless $B \rightarrow PV$ decays with $\Delta S = 0$. The captions are the same as in Table 1.

Decay Modes	NF	$\bar{\mathcal{B}}^f$		$\bar{\mathcal{B}}^{f+a}$		Experiment
		$\mathcal{O}(\alpha_s)$	$\mathcal{O}(\alpha_s + \alpha_s^2)$	$\mathcal{O}(\alpha_s)$	$\mathcal{O}(\alpha_s + \alpha_s^2)$	
$B^- \rightarrow \pi^- \rho^0$	8.04	7.34	7.24	7.31	7.22	$8.7^{+1.0}_{-1.1}$
$B^- \rightarrow \pi^0 \rho^-$	13.17	12.39	12.56	12.66	12.84	$10.8^{+1.4}_{-1.5}$
$\bar{B}^0 \rightarrow \pi^+ \rho^-$	18.61	18.40	18.74	19.34	19.69	$13.9^{+2.2}_{-2.1}$
$\bar{B}^0 \rightarrow \pi^- \rho^+$	9.67	9.54	9.56	10.08	10.10	$10.1^{+2.1}_{-1.9}$
$\bar{B}^0 \rightarrow \pi^\pm \rho^\mp$	28.28	27.94	28.30	29.42	29.79	24.0 ± 2.5
$\bar{B}^0 \rightarrow \pi^0 \rho^0$	0.44	0.34	0.31	0.26	0.24	$1.83^{+0.56}_{-0.55}$
$B^- \rightarrow \pi^- \omega$	7.12	6.53	6.69	6.30	6.45	6.6 ± 0.6
$\bar{B}^0 \rightarrow \pi^0 \omega$	0.017	0.015	0.021	0.005	0.005	< 1.2
$B^- \rightarrow K^- K^{*0}$	0.16	0.19	0.27	0.26	0.36	< 5.3
$\bar{B}^0 \rightarrow \bar{K}^0 K^{*0}$	0.14	0.17	0.25	0.24	0.32	...
$B^- \rightarrow K^0 K^{*-}$	0.04	0.07	0.05	0.18	0.14	...
$\bar{B}^0 \rightarrow K^0 \bar{K}^{*0}$	0.04	0.06	0.04	0.17	0.14	...
$\bar{B}^0 \rightarrow K^{*-} K^+$	0.02
$\bar{B}^0 \rightarrow K^- K^{*+}$	0.02
$B^- \rightarrow \pi^- \phi$	0.001	0.008	< 0.41
$\bar{B}^0 \rightarrow \pi^0 \phi$	0.0004	0.0035	< 1.0

are sensitive to the angle γ .

- The decays $B \rightarrow K\rho$ and $B \rightarrow K\omega$. The predicted CP -averaged branching ratios of these decay modes are also lower than the experimental data. In these decay channels, the dominant penguin coefficient is $\alpha_4^p(VP) = a_4^p(VP) - r_\chi^p a_6^p(VP)$. Since both the vector penguin coefficient $a_4^p(VP)$ and the scalar penguin coefficient $a_6^p(VP)$ are negative, the destruction between them reduce $\alpha_4^p(VP)$ very much. The branching ratios of these modes are therefore significantly smaller than those of the corresponding $B \rightarrow PP$ counterparts. It also makes the sub-leading corrections important to account for the ex-

perimental data. However, after the inclusion of the next-to-next leading order penguin contraction contributions, the branching ratios of these decay channels will be decreased by about $20\% \sim 30\%$. The weak annihilation contributions, however, tend to increase the branching ratios significantly, which are very crucial for explaining the current measured data.

For $\Delta S = 0$ decays, since the $b \rightarrow d$ penguin contribution is suppressed by the CKM factor λ'_t compared to the $b \rightarrow s$ penguin, most of them are dominated by the tree amplitudes, however, with a few exceptions. Considering the large uncertainties in the experimental data on these CP -averaged branching ratios, the theoretical predictions for most decay modes are roughly consistent with the data. Some general remarks are in order.

- The decays $\bar{B}^0 \rightarrow \pi^\pm \rho^\mp$ and $B^- \rightarrow \pi^0 \rho^-, \pi^- \rho^0, \pi^- \omega$. These decay channels are dominated by the tree amplitudes and depend mainly on the large coefficient α_1 , which receives small radiative corrections. Thus, there are no large differences between the predictions of the QCDF approach and those of the NF approximation. Both the weak annihilation contributions and the higher order penguin contraction contributions are small for these decay channels.
- The decays $\bar{B}^0 \rightarrow \pi^0 \rho^0$ and $\bar{B}^0 \rightarrow \pi^0 \omega$. Since these decay channels are dominated by the tree coefficient α_2 , which is far smaller than the coefficient α_1 , they are predicted to have smaller branching ratios. The higher order penguin contraction contributions are always smaller than the weak annihilation contributions. In addition, because of $\pi^0(\rho^0) = \frac{\bar{u}u - \bar{d}d}{\sqrt{2}}$ and $\omega = \frac{\bar{u}u + \bar{d}d}{\sqrt{2}}$, a large destructive interference occurs in the decay amplitudes of the decay $\bar{B}^0 \rightarrow \pi^0 \omega$, explaining why $\bar{B}r(\bar{B}^0 \rightarrow \pi^0 \omega) \ll \bar{B}r(\bar{B}^0 \rightarrow \pi^0 \rho^0)$. By the same reason, both the weak annihilation and the higher order penguin contraction contributions play a more important role in the $\pi^0 \omega$ mode than in the $\pi^0 \rho^0$ mode.
- The decays $B^- \rightarrow K^- K^{*0}$ and $\bar{B}^0 \rightarrow \bar{K}^0 K^{*0}$. These decay channels are dominated by the $b \rightarrow d$ penguin transition. In their decay amplitudes, the dominant terms are proportional to the coefficient $\alpha_4^p(PV)$. Analogous to the discussions of the decays $B \rightarrow \pi K^*$, we find that the weak annihilation contributions and the higher order penguin contraction contributions can increase their branching ratios by about $40\% \sim 50\%$. The penguin

coefficients are, however, strongly suppressed by the CKM factor $|\lambda'_t/\lambda_t| \sim 0.2$. The branching ratios of these decay modes are therefore smaller than those of the decays $B \rightarrow \pi K^*$.

- The decays $B^- \rightarrow K^0 K^{*-}$ and $\overline{B}^0 \rightarrow K^0 \overline{K}^{*0}$. These decay channels are also dominated by the $b \rightarrow d$ penguin transition. The dominant contributions to the decay amplitudes are, however, proportional to $\alpha_4^p(VP)$. Due to the delicate cancellations among various competing terms, their branching ratios are relatively small. This also renders the weak annihilation contributions to these decay channels potentially large. The higher order penguin contraction corrections interfere destructively with the normal QCDF results and will decrease the branching ratios by about 30%. In addition, it should be noted that since $\alpha_4^c \approx \alpha_4^u$ and $|\lambda'_u| \approx |\lambda'_c|$, large interference effects exist between these two terms, the branching ratios of these $b \rightarrow d$ penguin dominated decay modes have a strong dependence on the weak angle γ .
- The decays $\overline{B}^0 \rightarrow K^+ K^{*-}, K^- K^{*+}$. These two decay channels are pure annihilation processes. Studying on these decay modes may be helpful to learn more about the strength of annihilation contribution and to provide some useful information about final state interactions. Their branching ratios can hardly be affected by the higher order penguin contraction contributions.
- The decays $B^- \rightarrow \pi^- \phi$ and $\overline{B}^0 \rightarrow \pi^0 \phi$. These two decay channels do not receive the weak annihilation contributions and are pure penguin processes. Due to the small coefficients $\alpha_3^p(\pi\phi)$ and $\alpha_{3,ew}^p(\pi\phi)$, the branching ratios of these decay channels are quite small. From the numerical results, we can see that the “nonfactorizable” contributions dominate these decays. The higher order penguin contraction contributions have negligible impact on these decay channels.

From the above discussions, we can see that the higher order penguin contractions of the spectator-scattering amplitudes play an important role in penguin-dominated $B \rightarrow PV$ decays, while for tree-dominated $B \rightarrow PV$ decays, their effects are usually quite small. In particular, for decay modes dominated by the coefficient $\alpha_4^p(PV)$, these higher order penguin contraction contributions can increase the branching ratios by about 30% \sim 70%, while for the opposite

Table 3: The direct CP -violating asymmetries (in units of 10^{-2}) for hadronic charmless $B \rightarrow PV$ decays with $\Delta S = 1$. \mathcal{A}_{CP}^f and \mathcal{A}_{CP}^{f+a} denote the results without and with the annihilation contributions, respectively.

Decay Modes	\mathcal{A}_{CP}^f		\mathcal{A}_{CP}^{f+a}		Experiment
	$\mathcal{O}(\alpha_s)$	$\mathcal{O}(\alpha_s + \alpha_s^2)$	$\mathcal{O}(\alpha_s)$	$\mathcal{O}(\alpha_s + \alpha_s^2)$	
$B^- \rightarrow \pi^- \bar{K}^{*0}$	1.36	1.15	1.06	0.92	-9.3 ± 6.0
$B^- \rightarrow \pi^0 K^{*-}$	12.49	12.10	9.92	9.74	4 ± 29
$\bar{B}^0 \rightarrow \pi^+ K^{*-}$	8.37	8.92	5.74	6.37	-5 ± 14
$\bar{B}^0 \rightarrow \pi^0 \bar{K}^{*0}$	-9.88	-7.65	-7.19	-5.94	-1^{+27}_{-26}
$B^- \rightarrow \bar{K}^0 \rho^-$	0.41	0.46	0.25	0.27	...
$B^- \rightarrow K^- \rho^0$	-6.15	-9.06	-6.40	-8.55	31^{+12}_{-11}
$\bar{B}^0 \rightarrow K^- \rho^+$	-1.33	-3.54	-0.35	-1.31	17^{+15}_{-16}
$\bar{B}^0 \rightarrow \bar{K}^0 \rho^0$	9.43	10.80	6.71	7.37	...
$B^- \rightarrow K^- \omega$	-4.08	-5.52	-3.87	-4.81	2 ± 7
$\bar{B}^0 \rightarrow \bar{K}^0 \omega$	-10.41	-12.45	-7.14	-8.04	44 ± 23
$B^- \rightarrow K^- \phi$	1.85	1.53	1.38	1.18	3.7 ± 5.0
$\bar{B}^0 \rightarrow \bar{K}^0 \phi$	1.85	1.53	1.45	1.24	9 ± 14

case where the decay amplitudes are dominated by the coefficient $\alpha_4^p(VP)$, the branching ratios will be decreased by about $20\% \sim 30\%$ after the inclusion of these higher order contributions.

3.2 Direct CP -violating asymmetries of $B \rightarrow PV$ decays

As is well-known that the CP violation and the quark mixing parameters are closely related to each other in the SM. Studies on the CP asymmetries can therefore provide additional information about the flavor parameters of the SM. In this subsection, we will discuss the direct CP -violating asymmetries of the hadronic charmless $B \rightarrow PV$ decays with the QCDF approach. In particular, we will investigate the impact of penguin contractions of the spectator-scattering amplitudes on this quantity.

Here we adopt the standard “ \bar{B} minus B ” convention for the direct CP -violating asymme-

Table 4: The direct CP -violating asymmetries (in units of 10^{-2}) for hadronic charmless $B \rightarrow PV$ decays with $\Delta S = 0$. We do not consider the decay modes $B \rightarrow \pi\phi$ and $\bar{B}^0 \rightarrow K^\pm K^{*\mp}$, since their branching ratios are much smaller. The captions are the same as in Table 3.

Decay Modes	\mathcal{A}_{CP}^f		\mathcal{A}_{CP}^{f+a}		Experiment
	$\mathcal{O}(\alpha_s)$	$\mathcal{O}(\alpha_s + \alpha_s^2)$	$\mathcal{O}(\alpha_s)$	$\mathcal{O}(\alpha_s + \alpha_s^2)$	
$B^- \rightarrow \pi^- \rho^0$	3.32	4.28	3.94	4.91	-7^{+12}_{-13}
$B^- \rightarrow \pi^0 \rho^-$	-2.33	-2.94	-2.66	-3.25	1 ± 11
$\bar{B}^0 \rightarrow \pi^+ \rho^-$	-1.08	-1.53	-1.05	-1.49	-15 ± 9
$\bar{B}^0 \rightarrow \pi^- \rho^+$	0.33	0.63	0.20	0.49	-47^{+13}_{-14}
$\bar{B}^0 \rightarrow \pi^0 \rho^0$	-4.50	3.86	-14.65	-4.73	-49^{+70}_{-83}
$B^- \rightarrow \pi^- \omega$	-2.35	-3.09	-2.14	-2.91	6.6 ± 0.6
$\bar{B}^0 \rightarrow \pi^0 \omega$	-26.93	-51.13	59.79	-63.50	4 ± 8
$B^- \rightarrow K^- K^{*0}$	-34.79	-29.27	-28.55	-24.56	...
$\bar{B}^0 \rightarrow \bar{K}^0 K^{*0}$	-34.79	-29.27	-29.78	-25.56	...
$B^- \rightarrow K^0 K^{*-}$	-11.14	-13.01	-6.79	-7.61	...
$\bar{B}^0 \rightarrow K^0 \bar{K}^{*0}$	-11.14	-13.02	-6.82	-7.43	...

try [19, 43]

$$\mathcal{A}_{CP} \equiv \frac{\mathcal{Br}(\bar{B}^0 \rightarrow \bar{f}) - \mathcal{Br}(B^0 \rightarrow f)}{\mathcal{Br}(\bar{B}^0 \rightarrow \bar{f}) + \mathcal{Br}(B^0 \rightarrow f)}, \quad (43)$$

in terms of the branching ratios. Our numerical results of the CP -violating asymmetries for charmless $B \rightarrow PV$ decays are listed in Tables 3 and 4. The parameters \mathcal{A}_{CP}^f and \mathcal{A}_{CP}^{f+a} denote the predictions without and with the weak annihilation contributions, respectively. Some remarks are as follows.

- The direct CP -violating asymmetries of most $B \rightarrow PV$ decays are predicted to be typically small within the QCDF formalism. This could be well understood, since the direct CP -violating asymmetries are proportional to the sines of the strong interaction phase shifts between two contributing amplitudes with both different weak and strong phases, which are usually suppressed by α_s and/or Λ_{QCD}/m_b within the QCDF formalism. This is

particularly true for decay modes with only one dominating decay amplitude, for example, the decays $\overline{B}^0 \rightarrow \pi^- \rho^+$ and $B^- \rightarrow \overline{K}^0 \rho^-$.

- Since the coefficients α_2 and α_4^p can receive a large imaginary part from the “nonfactorizable” contributions with the QCDF approach, there might be large direct CP -violating asymmetries for those α_2 and α_4^p dominant decay modes. In addition, the direct CP -violating asymmetries for these decay modes are usually strongly affected by the weak annihilation contributions. For example, the decays $B^- \rightarrow \pi^0 K^{*-}$ and $\overline{B}^0 \rightarrow \pi^0 \omega$ belong to this category.
- Although the individual Feynman diagram in Fig. 6 carries large strong phase, the combining contributions of these higher order diagrams contain only a relatively small one. Thus, these higher order penguin contraction contributions to the direct CP -violating asymmetries for most $B \rightarrow PV$ decays are also small, but with a few exceptions discussed below.
- From Table 4, we can see that the higher order penguin contraction contributions have significant effects on the direct CP -violating asymmetries of the decays $\overline{B}^0 \rightarrow \pi^0 \rho^0$ and $\overline{B}^0 \rightarrow \pi^0 \omega$, even changing the sign of those predicted at next-to-leading order in α_s . This is due to the delicate cancellations among the competing terms in their decay amplitudes, making these higher order penguin contraction contributions potentially large. In addition, the annihilation contributions have also significant effects on the direct CP -violating asymmetries of these decay modes, but with opposite signs.
- From the numerical results listed in Tables 3 and Table 4, we can see that the higher order penguin contraction contributions to the direct CP -violating asymmetries of penguin-dominated $B \rightarrow PV$ decays usually obey the following general rules: for decay modes dominated by the coefficient $\alpha_4^p(PV)$, the higher order contributions will decrease the direct CP -violating asymmetries, while for the opposite case where the decay amplitudes are dominated by the coefficient $\alpha_4^p(VP)$, the direct CP -violating asymmetries will be increased after the inclusion of these higher order contributions. In addition, the weak annihilation contributions in the latter case are more important than in the former, due

to the destructive interference between the QCD penguin coefficients a_4^p and a_6^p appearing in the coefficient $\alpha_4^p(VP)$.

- In the $b \rightarrow d$ penguin dominated decays $B \rightarrow KK^*$, the penguin amplitudes generated by the internal u quark are no longer suppressed by the CKM factors, large interference effects between various terms contributing to the decay amplitudes are expected. Thus, large direct CP -violating asymmetries for these decay channels are predicted with the QCDF approach.

Although the direct CP -violating asymmetries of some hadronic charmless $B \rightarrow PV$ decay channels have been measured recently, the data are still too uncertain to draw any conclusions from the comparison with the theoretical predictions. With a rapid accumulation of the experimental data, large direct CP -violating asymmetries of some decay channels, for example, the decays $B \rightarrow KK^*$, are expected to be found in the near future.

3.3 Detailed analysis of $B \rightarrow \pi K^*$, $K\rho$ decays

The $B \rightarrow \pi K^*$ and $B \rightarrow K\rho$ decays, like their PP counterparts $B \rightarrow \pi K$ decays, are also penguin-dominated decay modes and therefore sensitive to new physics contributions. With the improvement of the measurements, if the “ πK ” puzzles remain still unexplainable within the SM, there would be signals of some new physics beyond the SM [44]. Thus, the $B \rightarrow \pi K^*$ and $B \rightarrow K\rho$ decays can be used to determine whether there are any new physics contributions, and which one, if exist as hinted by “ πK ” puzzles, is more favored. In addition, these decay modes can also be used to extract the weak angle γ [45]. So, detailed studies on these decay modes are worthy.

In Figs. 9 and 10, we show the dependence of the CP -averaged branching ratios of these decay modes on the weak phase γ , where the solid and the dashed lines correspond to the theoretical predictions with and without the higher order penguin contraction contributions, respectively. The horizontal solid lines denote the experimental data as given in Table 1, with the thicker one denoting its center value and the thinner ones its error bars. The NF results denoted by the dash-dotted lines are also shown for comparison. In these and the following figures, the default values of all input parameters except for the CKM angle γ are used.

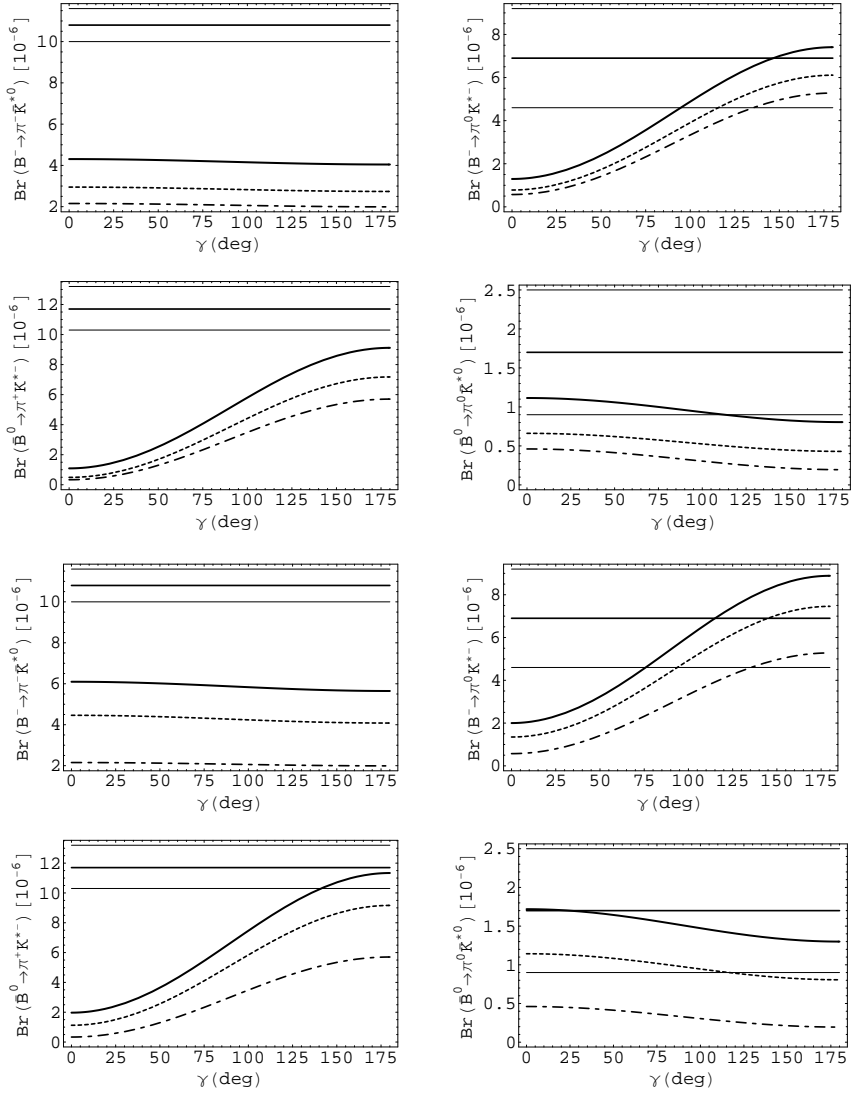


Figure 9: The γ dependence of the CP -averaged branching ratios for $B \rightarrow \pi K^*$ decays. The upper four and the lower four plots denote the results without and with the annihilation contributions, respectively. The solid and the dashed lines correspond to the theoretical predictions with and without the penguin contraction, respectively. The horizontal solid lines denote the experimental data as given in Table 1, with the thicker ones being its center values and the thinner its error bars. The NF results denoted by the dash-dotted lines are also shown for comparison.

From these two figures and the numerical results given by Table 1, we can see that the experimental data on these decay modes are usually larger than the theoretical predictions;

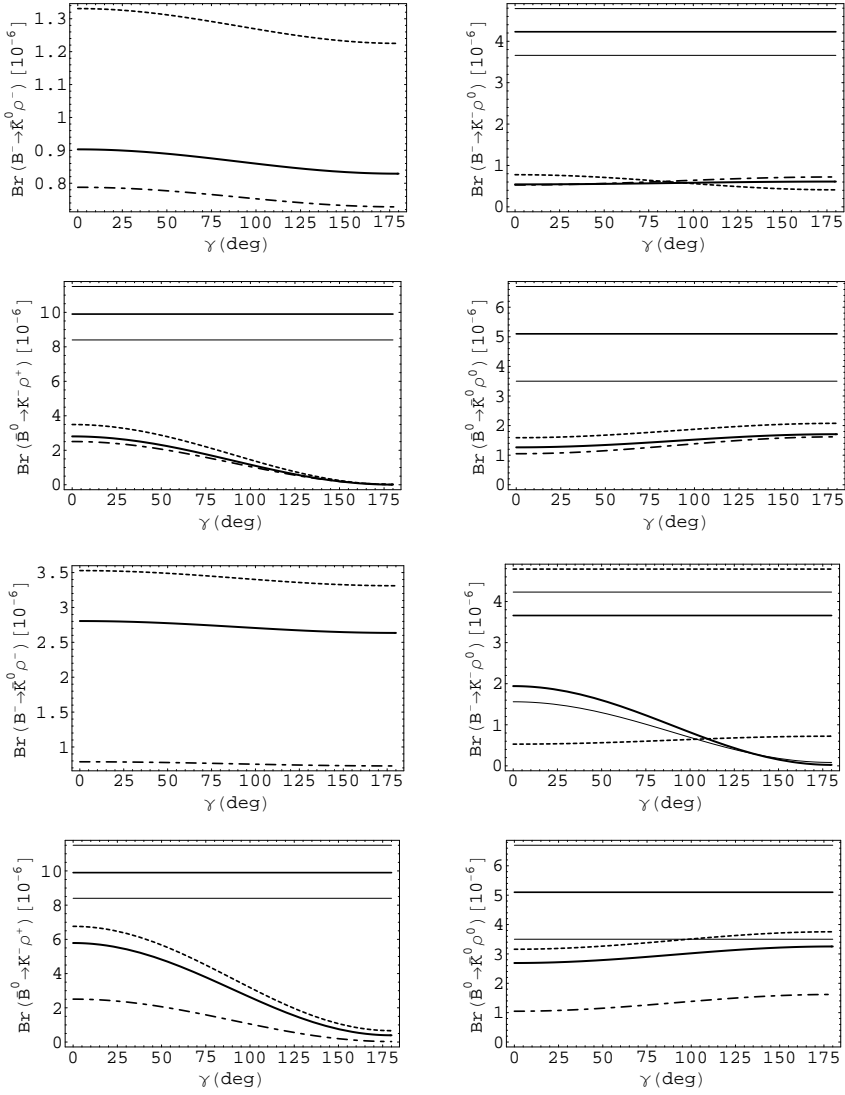


Figure 10: The same as Fig. 9 but for $B \rightarrow K\rho$ decays.

Some decay modes, for example, the $B^- \rightarrow \pi^0 K^{*-}$ decay, do have a strong dependence on the angle γ ; In addition, the higher order penguin contraction contributions can give a significant enhancement to the CP -averaged branching ratios of $B \rightarrow \pi K^*$ decays, while decrease those of $B \rightarrow K^* \rho$ decays by about 20% \sim 30%.

Since the uncertainties in the predictions of the branching ratios can be largely eliminated by taking ratios between them, in the following we will discuss some ratios between the branching fractions of these decay modes, like the ones defined for $B \rightarrow \pi K$ decays [46].

For $B \rightarrow \pi K^*$ decays, we define the following three ratios between the CP -averaged branch-

Table 5: Ratios between the CP -averaged branching fractions for $B \rightarrow \pi K^*, K\rho$ decays. The values in the parentheses are the ones without the annihilation contributions.

	NF	$\mathcal{O}(\alpha_s)$	$\mathcal{O}(\alpha_s + \alpha_s^2)$	Exp .
$R(\pi K^*)$	0.84	0.76 (0.79)	0.77 (0.77)	1.18 ± 0.17
$R_c(\pi K^*)$	1.52	1.29 (1.42)	1.22 (1.31)	1.28 ± 0.44
$R_n(\pi K^*)$	1.84	1.44 (1.72)	1.31 (1.45)	3.44 ± 1.68
$R(\rho K)$	2.70	1.65 (2.21)	1.77 (2.60)	> 0.22
$R_c(\rho K)$	1.48	0.85 (1.05)	0.87 (1.26)	> 0.18
$R_n(\rho K)$	0.77	0.80 (0.78)	0.79 (0.78)	0.97 ± 0.34

ing fractions [45]

$$R(\pi K^*) \equiv \frac{\tau_{B_u} \bar{\mathcal{B}}r(\bar{B}^0 \rightarrow \pi^+ K^{*-})}{\tau_{B_d} \bar{\mathcal{B}}r(B^- \rightarrow \pi^- \bar{K}^{*0})}, \quad (44)$$

$$R_c(\pi K^*) \equiv 2 \frac{\bar{\mathcal{B}}r(B^- \rightarrow \pi^0 K^{*-})}{\bar{\mathcal{B}}r(B^- \rightarrow \pi^- \bar{K}^{*0})}, \quad (45)$$

$$R_n(\pi K^*) \equiv \frac{1}{2} \frac{\bar{\mathcal{B}}r(\bar{B}^0 \rightarrow \pi^+ K^{*-})}{\bar{\mathcal{B}}r(\bar{B}^0 \rightarrow \pi^0 \bar{K}^{*0})}. \quad (46)$$

Substituting the $\rho(K)$ meson for the $\pi(K^*)$ meson, we can get another three similar quantities corresponding to $B \rightarrow K\rho$ decays. The theoretical predictions and the current experimental data of these ratios are collected in Table 5. For the γ dependence of these quantities, we display them in Figs. 11 and 12, where the lines have the same interpretations as in Fig. 9.

From these two figures and the numerical results given in Table 5, we can see that:

- Considering the large uncertainties in the experimental data, our theoretical predictions for most of these ratios are roughly consistent with the data. From the γ dependence of these ratios, the preferred value of this phase is also consistent with that given in [50].
- Since these ratios are usually dependent of fewer input parameters, large uncertainties, for example, related to the heavy-to-light form factors, can be eliminated in these quantities. Thus, they are more appropriate to derive information about the weak phase γ as well as the tree and the penguin coefficients. Furthermore, compared to their PP counterparts,

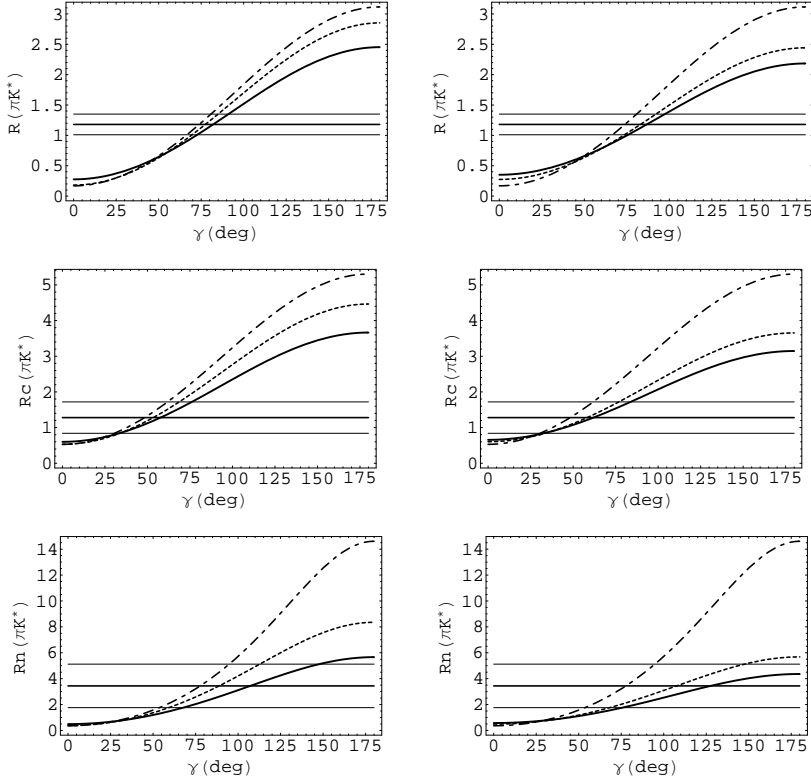


Figure 11: Ratios of the CP -averaged branching fractions for $B \rightarrow \pi K^*$ decays defined by Eqs. (44)–(46) as functions of the weak phase γ . The left and the right plots denote the results without and with the annihilation contributions, respectively. The meaning of the other lines is the same as in Fig. 9.

the leading penguin contributions in these PV modes are usually smaller due to either power suppressions or delicate cancellations among the vector and the scalar penguin coefficients $a_{4,6}^p$. Thus, sub-leading contributing amplitudes, for example, the weak annihilation contributions, will become relatively important. The numerical values in the $K\rho$ modes confirm this point.

- From the explicit expressions of the decay amplitudes for these decay modes [19], we can see that differences between the two ratios R_c and R_n for both πK^* and $K\rho$ modes arise mainly from the color-allowed electro-weak penguin coefficient $\alpha_{3,ew}^p$, which are predicted to be small. The two ratios R_c and R_n are therefore expected to be approximately equal within the SM. However, due to the delicate cancellations among various competing terms,

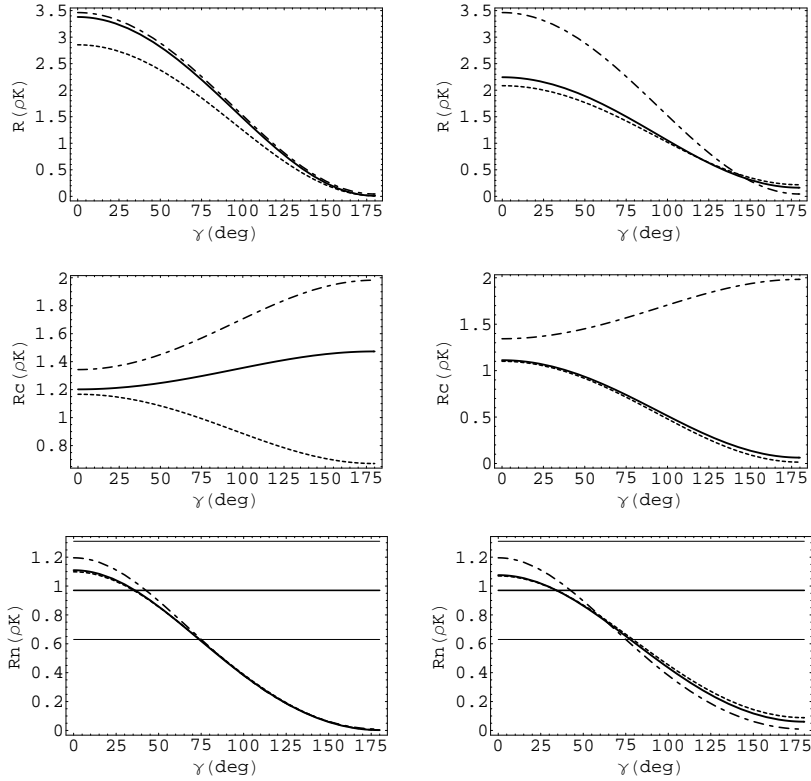


Figure 12: The same as Fig. 11 but for $B \rightarrow K\rho$ decays

these ratios are strongly affected by the sub-leading, in particular, the weak annihilation terms. After including the annihilation contributions, the two ratios R_c and R_n are indeed approximately equal. The current data, however, indicate that $R_n(\pi K^*)$ is somewhat larger than $R_c(\pi K^*)$, but with large uncertainties. Unfortunately, due to the insufficient data on the branching ratios of the $K\rho$ decays, direct experimental comparison between $R_c(\rho K)$ and $R_n(\rho K)$ is not feasible. Once the experimental “ $R_c - R_n$ ” comparison in the case of πK^* and $K\rho$ decays are available, we can determine whether our theoretical predictions based on the QCDF approach are correct.

- As the higher order penguin contraction contributions are similar in nature, and hence eliminated in the ratios between the corresponding branching fractions, the patterns of these quantities remain nearly unaffected even after these higher order contributions are included.

With refined measurements available in the coming years, it would be very interesting to

check whether the theoretical predictions for these ratios are consistent with the data. In addition, studies on these $B \rightarrow PV$ modes can help us to understand the “ πK ” puzzles [44].

4 Conclusions

In this paper, we have reexamined the hadronic charmless $B \rightarrow PV$ decays (with $P = (\pi, K)$, and $V = (\rho, K^*, \omega, \phi)$) within the framework of the QCDF, taking into account the penguin contractions of the spectator-scattering amplitudes induced by the $b \rightarrow Dg^*g^*$ transition, which are of order α_s^2 . The main conclusions of this paper are summarized as following.

1. For penguin-dominated $B \rightarrow PV$ decays, predictions of the QCDF approach are usually quite different from the ones obtained by the NF approximation due to large “nonfactorizable” effects on the penguin coefficients. Contrary to their PP counterparts, the PV modes usually have smaller dominant penguin coefficients α_4^p , rendering the sub-dominant terms potentially large. For example, the weak annihilation contributions, though power suppressed in the QCDF approach, are important in these penguin-dominated decay modes. In addition, the higher order penguin contraction contributions can interfere with the α_s order results constructively or destructively, and hence are also significant for these decay modes. In particular, for decay modes in which the spectator quark goes to the pseudoscalar meson in the final states, i.e., decay modes dominated by the coefficient $\alpha_4^p(PV)$, these higher order penguin contraction contributions can increase the CP -averaged branching ratios by about $30\% \sim 70\%$, while for the opposite case where the decay amplitudes are dominated by the coefficient $\alpha_4^p(VP)$, the branching ratios will be decreased by about $20\% \sim 30\%$ after the inclusion of these higher order contributions.
2. For either tree-dominated decays, or the decay channels having only the penguin coefficients α_3^p , $\alpha_{3,ew}^p$ or having only the weak annihilation contributions, the higher order penguin contraction contributions to the CP -averaged branching ratios are very small.
3. Since the direct CP -violating asymmetries are proportional to the sine of the strong interaction phase, which is usually suppressed by α_s and/or Λ_{QCD}/m_b within the QCDF formalism, most of the charmless $B \rightarrow PV$ decays are predicted to have typically small

direct CP -violating asymmetries. But, for those decay modes where there are large interference effects between various contributing decay amplitudes, large direct CP -violating asymmetries are predicted with the QCDF approach.

4. Because of large cancellations among the higher order penguin contraction contributions, only a relatively small strong phase remains. Thus, these higher order penguin contraction contributions to the direct CP -violating asymmetries for most $B \rightarrow PV$ decays are also small, but with a few exceptions. In the decays $\bar{B}^0 \rightarrow \pi^0 \rho^0$ and $\bar{B}^0 \rightarrow \pi^0 \omega$, because of the delicate cancellations among the competing terms in their decay amplitudes, these higher order penguin contraction contributions have significant effects on the direct CP -violating asymmetries. In addition, the higher order penguin contraction contributions to the direct CP -violating asymmetries of penguin-dominated $B \rightarrow PV$ decays usually obey the following general rules: for decay modes dominated by the coefficient $\alpha_4^p(PV)$, the higher order contributions will decrease the direct CP -violating asymmetries, while for the opposite case where the decay amplitudes are dominated by the coefficient $\alpha_4^p(VP)$, the direct CP -violating asymmetries will be increased after the inclusion of these higher order contributions.
5. With more accurate experimental results available in the coming years, it would be very interesting to check whether the theoretical predictions for the ratios R , R_c , and R_n for both the πK^* and the $K \rho$ decay modes are consistent with the experimental data. In particular, the experimental $R_c - R_n$ comparison with the case of πK^* and ρK decays are very crucial for our understandings of the “ πK ” puzzles.

Although the theoretical results presented here still have large uncertainties, the penguin contractions of the spectator-scattering amplitudes induced by the $b \rightarrow Dg^*g^*$ transition, which are of order α_s^2 , have been shown to be very important for the hadronic charmless $B \rightarrow PV$ decays, particularly for the penguin-dominated decay modes. It is very interesting to note that the 1-loop (α_s^2) correction to the hard spectator scattering in the tree-dominated $B \rightarrow \pi\pi$ decays has been performed recently [47], which forms another part of the NNLO contribution to the QCD factorization formula for hadronic B -meson decays. As for PQCD, NLO corrections have been carried out for $B \rightarrow \pi\pi, \pi K$ and $\rho\rho$ decays[61] very recently. With the steady

progress in experimental measurements at BABAR and Belle, further systematic studies on these higher order contributions to the rare hadronic B -meson decays are therefore interesting and deserving.

Acknowledgments

We thank Prof. Y.B. Dai for helpful discussions. The work is supported by National Science Foundation under contract No. 10305003, Henan Provincial Foundation for Prominent Young Scientists under contract No. 0312001700 and the NCET Program sponsored by Ministry of Education, China.

APPENDIX A: ANALYTIC EXPRESSIONS FOR THE Δ_i FUNCTIONS

In the NDR scheme, after performing the loop-momentum integration, subtracting the regulator ϵ using the $\overline{\text{MS}}$ scheme, and performing the Feynman parameter integrals, we get the analytic expressions of the Δ_i functions appearing in Eqs. (36) and (37) as

$$\begin{aligned} \Delta i_2 &= -\frac{22}{9} + \frac{8}{3} \ln \frac{\mu}{m_c} - \frac{2(8+r_1)}{3r_3} G_0(r_1) + \frac{2(8+r_1-2r_3)}{3r_3} G_0(r_1+r_3) \\ &\quad + \frac{4}{r_3} [G_{-1}(r_1) - G_{-1}(r_1+r_3)], \end{aligned} \quad (47)$$

$$\begin{aligned} \Delta i_3 &= \frac{22}{9} + \frac{12}{r_3} + \frac{4r_1}{3r_3} - \frac{8}{3} \ln \frac{\mu}{m_c} - \frac{2(7r_1-r_3-3r_1r_3+2r_1^2-2r_3^2)}{3r_3^2} G_0(r_1+r_3) \\ &\quad + \frac{2r_1(7+2r_1-3r_3)}{3r_3^2} G_0(r_1) - \frac{4(2r_1+r_3)}{r_3^2} [G_{-1}(r_1) - G_{-1}(r_1+r_3)] \\ &\quad + \frac{3(4-r_1)r_1}{r_3^2} T_0(r_1) - \frac{3(4-r_1-r_3)(r_1+r_3)}{r_3^2} T_0(r_1+r_3), \end{aligned} \quad (48)$$

$$\Delta i_8 = \frac{32}{9} - \frac{16}{3} \ln \frac{\mu}{m_c} - \frac{8(2+r_1)}{3r_3} G_0(r_1) + \frac{8(2+r_1+r_3)}{3r_3} G_0(r_1+r_3), \quad (49)$$

$$\begin{aligned} \Delta i_{12} &= -\frac{32}{9} + \frac{12}{r_3} + \frac{4r_1}{3r_3} + \frac{16}{3} \ln \frac{\mu}{m_c} + \frac{2r_1(7+2r_1+6r_3)}{3r_3^2} G_0(r_1) \\ &\quad - \frac{2(2r_1^2-r_3(1-4r_3)+r_1(7+6r_3))}{3r_3^2} G_0(r_1+r_3) \end{aligned}$$

$$\begin{aligned}
& -\frac{8 r_1}{r_3^2} [G_{-1}(r_1) - G_{-1}(r_1 + r_3)] + \frac{3 (4 - r_1) r_1}{r_3^2} T_0(r_1) \\
& -\frac{3 (4 - r_1 - r_3) (r_1 + r_3)}{r_3^2} T_0(r_1 + r_3)
\end{aligned} \tag{50}$$

$$\begin{aligned}
\Delta i_{17} = & \frac{2}{3} + \frac{2 (8 + r_1)}{3 r_3} G_0(r_1) - \frac{2}{3} \left(\frac{8 + r_1}{r_3} + \frac{4}{r_1 + r_3} \right) G_0(r_1 + r_3) \\
& -\frac{4}{r_3} [G_{-1}(r_1) - G_{-1}(r_1 + r_3)],
\end{aligned} \tag{51}$$

$$\begin{aligned}
\Delta i_{21} = & -\frac{2}{3} - \frac{16}{r_3} - \frac{8 r_1}{3 r_3} + \frac{2 r_1 (4 r_1^2 + 3 r_3 (8 + r_3) + r_1 (20 + 7 r_3))}{3 r_3^2 (r_1 + r_3)} G_0(r_1 + r_3) \\
& -\frac{2 r_1 (20 + 4 r_1 + 3 r_3)}{3 r_3^2} G_0(r_1) + \frac{4 (4 r_1 + r_3)}{r_3^2} [G_{-1}(r_1) - G_{-1}(r_1 + r_3)] \\
& -\frac{4 (4 - r_1) r_1}{r_3^2} T_0(r_1) + \frac{4 (4 - r_1 - r_3) (r_1 + r_3)}{r_3^2} T_0(r_1 + r_3),
\end{aligned} \tag{52}$$

where we have introduced the notations $r_1 = k^2/m_q^2$, $r_2 = p^2/m_q^2$ and $r_3 = 2(k \cdot p)/m_q^2$, with $m_q = m_c$ or m_b . For light u, d, s quark propagating in the fermion loops, these Δi functions can be evaluated straightforwardly. Here we give only the relevant Δi functions needed in this paper. The explicit expressions of the remaining ones can be obtained in a similar manner.

The functions $G_i(t)$ ($i = -1, 0$) are defined by

$$G_i(t) = \int_0^1 dx x^i \ln [1 - x (1 - x) t - i\delta], \tag{53}$$

and the explicit form for $G_{-1,0}(t)$ could be found in Ref. [26].

In addition, we have also defined the function $T_i(t)$, which is defined by

$$T_i(t) = \int_0^1 dx \frac{x^i}{1 - x (1 - x) t - i\delta}. \tag{54}$$

The explicit form for $T_0(t)$ is given by [28]

$$T_0(t) = \begin{cases} \frac{4 \arctan \sqrt{\frac{t}{4-t}}}{\sqrt{t(4-t)}}; & 0 \leq t \leq 4 \\ \frac{2i \pi + 2 \ln(\sqrt{t} - \sqrt{t-4}) - 2 \ln(\sqrt{t} + \sqrt{t-4})}{\sqrt{t(t-4)}}; & t > 4. \end{cases} \tag{55}$$

APPENDIX B: INPUT PARAMETERS

In this appendix, we present the relevant input parameters used in our numerical calculations as follows.

Wilson coefficients.—The Wilson coefficients $C_i(\mu)$ have been reliably evaluated to next-to-leading logarithmic order [36, 48]. Their numerical values in the NDR scheme at the scale $\mu = m_b$ ($\mu_h = \sqrt{\Lambda_h m_b}$) are given by

$$\begin{aligned} C_1 &= 1.080 \ (1.173), & C_2 &= -0.180 \ (-0.347), & C_3 &= 0.014 \ (0.028), \\ C_4 &= -0.035 \ (-0.062), & C_5 &= 0.009 \ (0.010), & C_6 &= -0.040 \ (-0.084), \\ C_7/\alpha_{\text{e.m.}} &= -0.009 \ (-0.025), & C_8/\alpha_{\text{e.m.}} &= 0.054 \ (0.109), & C_9/\alpha_{\text{e.m.}} &= -1.239 \ (-1.362), \\ C_{10}/\alpha_{\text{e.m.}} &= 0.224 \ (0.426), & C_{7\gamma}^{\text{eff}} &= -0.303 \ (-0.372), & C_{8g}^{\text{eff}} &= -0.145 \ (-0.172). \end{aligned} \tag{56}$$

with the input parameters fixed as [50]: $\alpha_s(m_Z) = 0.1187$, $\alpha_{\text{e.m.}}(m_W) = 1/129$, $m_W = 80.425$ GeV, $m_Z = 91.188$ GeV, $\sin^2 \theta_W = 0.2312$, $m_t = 178.1$ GeV, $m_b = 4.65$ GeV, $\Lambda_h = 0.5$ GeV.

The CKM matrix elements.—Here we use the Wolfenstein parametrization for the CKM matrix elements [49]

$$V_{\text{CKM}} = \begin{pmatrix} 1 - \frac{\lambda^2}{2} & \lambda & A\lambda^3(\rho - i\eta) \\ -\lambda & 1 - \frac{\lambda^2}{2} & A\lambda^2 \\ A\lambda^3(1 - \rho - i\eta) & -A\lambda^2 & 1 \end{pmatrix} + \mathcal{O}(\lambda^4), \tag{57}$$

and choose the four Wolfenstein parameters (A , λ , ρ , and η) as

$$A = 0.8533, \quad \lambda = 0.2200, \quad \bar{\rho} = 0.20, \quad \bar{\eta} = 0.33, \tag{58}$$

with $\bar{\rho}$ and $\bar{\eta}$ defined by $\bar{\rho} = \rho(1 - \frac{\lambda^2}{2})$, $\bar{\eta} = \eta(1 - \frac{\lambda^2}{2})$.

Masses and lifetimes.—For the quark mass, there are two different classes appearing in the QCDF approach. One type is the pole quark mass which appears in the evaluation of the penguin loop corrections, and is denoted by m_q . In this paper, we take

$$m_u = m_d = m_s = 0, \quad m_c = 1.46 \text{ GeV}, \quad m_b = 4.65 \text{ GeV}. \tag{59}$$

The other one is the current quark mass which appears in the factor r_χ^M . This kind of quark mass is scale dependent. Following Ref. [19], we hold $(\overline{m}_u + \overline{m}_d)(\mu)/\overline{m}_s(\mu)$ fixed and use $\overline{m}_s(\mu)$ as an input parameter [50]

$$\begin{aligned} \overline{m}_u(2 \text{ GeV}) &= \overline{m}_d(2 \text{ GeV}) = 0.04 \overline{m}_s(2 \text{ GeV}), \\ \overline{m}_s(2 \text{ GeV}) &= 105 \text{ MeV}, \quad \overline{m}_b(\overline{m}_b) = 4.26 \text{ GeV}. \end{aligned} \tag{60}$$

where the difference between the u and d quark is not distinguished.

For the lifetimes and the masses of the B mesons, we adopt the center values given by [50]

$$\tau_{B_u} = 1.671 \text{ ps}, \quad \tau_{B_d} = 1.536 \text{ ps}, \quad m_{B_u} = 5.2794 \text{ GeV}, \quad m_{B_d} = 5.2790 \text{ GeV}, \quad (61)$$

The masses of the light mesons are also chosen from Ref. [50].

Light-cone distribution amplitudes (LCDAs) of mesons.—The LCDAs of mesons are also basic input parameters in the QCDF approach. In the heavy quark limit, the light-cone projectors for the B , the pseudoscalar, and the vector mesons in the momentum space can be expressed, respectively, as [3, 19]

$$\mathcal{M}_{\alpha\beta}^B = -\frac{if_B m_B}{4} \left[(1 + \not{p}) \gamma_5 \left\{ \Phi_1^B(\xi) + \not{\mu}_- \Phi_2^B(\xi) \right\} \right]_{\alpha\beta}, \quad (62)$$

$$M_{\alpha\beta}^P = \frac{if_P}{4} \left[\not{p} \gamma_5 \Phi_P(x) - \mu_P \gamma_5 \frac{\not{k}_2 \not{k}_1}{\not{k}_1 \cdot \not{k}_2} \Phi_p(x) \right]_{\alpha\beta}, \quad (63)$$

$$(M_{\parallel}^V)_{\alpha\beta} = -\frac{if_V}{4} \left[\not{p} \Phi_V(x) - \frac{m_V f_V^\perp}{f_V} \frac{\not{k}_2 \not{k}_1}{\not{k}_1 \cdot \not{k}_2} \Phi_v(x) \right]_{\alpha\beta}, \quad (64)$$

where k_1 and k_2 are the quark and anti-quark momenta of the meson constituents and defined, respectively, by

$$k_1^\mu = xp^\mu + k_\perp^\mu + \frac{\vec{k}_\perp^2}{2xp \cdot \vec{p}} \vec{p}^\mu, \quad k_2^\mu = (1-x)p^\mu - k_\perp^\mu + \frac{\vec{k}_\perp^2}{2(1-x)p \cdot \vec{p}} \vec{p}^\mu. \quad (65)$$

It is understood that only after the factor $k_1 \cdot k_2$ in the denominator of Eqs. (63) and (64) cancelled, can we take the collinear approximation, i.e., the momentum k_1 and k_2 can be set to be xp and $(1-x)p$, respectively, with p being the momentum of the meson. $\Phi_M(x)$ and $\Phi_m(x)$ are the leading twist and twist-3 LCDAs of the meson M , respectively. Since the QCDF approach is based on the heavy quark assumption, to a very good approximation, we can use the asymptotic forms of the LCDAs [51, 54, 55]

$$\Phi_P(x) = \Phi_V(x) = 6x(1-x), \quad \Phi_p(x) = 1, \quad \Phi_v(x) = 3(2x-1). \quad (66)$$

With respect to the endpoint divergence associated with the momentum fraction integral over the LCDAs, following the treatment in Refs. [10, 56], we regulate the integral with an *ad-hoc* cut-off

$$\int_0^1 \frac{dx}{x} \rightarrow \int_{\Lambda_h/m_B}^1 \frac{dx}{x} = \ln \frac{m_B}{\Lambda_h}, \quad (67)$$

with $\Lambda_h = 500$ MeV. The possible complex phase associated with this integral has been neglected.

As for the B meson wave functions, we need only consider the first inverse moment of the LCDA $\Phi_1^B(\xi)$ defined by [10]

$$\int_0^1 \frac{d\xi}{\xi} \Phi_1^B(\xi) \equiv \frac{m_B}{\lambda_B}, \quad (68)$$

where the hadronic parameter λ_B has been introduced to parameterize this integral. In this paper, we take $\lambda_B = 460$ MeV as our default input value [57, 58].

Decay constants and transition form factors.— The decay constants and the form factors are nonperturbative parameters and can be determined from experiments and/or theoretical estimations, such as lattice calculations, QCD sum rules, etc. For their definitions, we refer the readers to Refs. [1, 51, 54]. In this paper, we take the following numerical values for these input parameters

$$\begin{aligned} f_\pi &= 130.7 \text{ MeV} [50], & f_K &= 159.8 \text{ MeV} [50], & f_B &= 180 \text{ MeV} [59], \\ f_\rho &= 205 \text{ MeV} [60], & f_\omega &= 195 \text{ MeV} [60], & f_{K^*} &= 217 \text{ MeV} [60], \\ f_\phi &= 231 \text{ MeV} [60], & f_\rho^\perp(1 \text{ GeV}) &= 160 \text{ MeV} [60], & f_\omega^\perp(1 \text{ GeV}) &= 145 \text{ MeV} [60], \\ f_{K^*}^\perp(1 \text{ GeV}) &= 185 \text{ MeV} [60], & f_\phi^\perp(1 \text{ GeV}) &= 200 \text{ MeV} [60], \\ F_1^{B \rightarrow \pi}(0) &= 0.258 [60], & F_1^{B \rightarrow K}(0) &= 0.331 [60], & A_0^{B \rightarrow \rho}(0) &= 0.303 [60], \\ A_0^{B \rightarrow K^*}(0) &= 0.374 [60], & A_0^{B \rightarrow \omega}(0) &= 0.281 [60]. \end{aligned}$$

where the form factors are evaluated at the maximal recoil region. The dependence of the form factors on the momentum-transfer q^2 can be found in Ref. [60]. It should be noted that the transverse decay constant f_V^\perp is scale dependent.

References

- [1] M. Bauer, B. Stech, and M. Wirbel, Z. Phys. C **29**, 637 (1985); Z. Phys. C **34**, 103 (1987).
- [2] T. W. Yeh and H-n. Li, Phys. Rev. D **56**, 1615 (1997). Y. Y. Keum, H-n. Li, and A. I. Sanda, Phys. Lett. B **504**, 6 (2001); Phys. Rev. D **63**, 054008 (2001); Y. Y. Keum and H-n. Li, Phys. Rev. D **63**, 074006 (2001).

- [3] M. Beneke, G. Buchalla, M. Neubert, C. T. Sachrajda, Phys. Rev. Lett. **83**, 1914 (1999); Nucl. Phys. B **591**, 313 (2000).
- [4] M. Neubert, AIP Conf. Proc. **602**, 168 (2001); AIP Conf. Proc. **618**, 217 (2002).
- [5] C. W. Bauer, D. Pirjol, and I. W. Stewart, Phys. Rev. Lett. **87**, 201806 (2001); Phys. Rev. D **65**, 054022 (2002); ibid. **67**, 071502 (2003); J. Chay and C. Kim, Phys. Rev. D **65**, 114016 (2002); M. Beneke, A. P. Chapovsky, M. Diehl, and T. Feldmann, Nucl. Phys. B **643**, 431 (2002).
- [6] Y. L. Wu and Y. F. Zhou, Phys. Rev. D **72**, 034037 (2005);
- [7] C. W. Chiang, M. Gronau, J. L. Rosner, and D. A. Suprun, Phys. Rev. D **70**, 034020 (2004).
- [8] C. W. Chiang, M. Gronau, Z. Luo, J. L. Rosner, and D. A. Suprun, Phys. Rev. D **69**, 034001 (2004).
- [9] Y. Y. Keum and H. n. Li, Phys. Rev. D **63**, 074006 (2001).
- [10] M. Beneke, G. Buchalla, M. Neubert and C. T. Sachrajda, Nucl. Phys. B **606**, 245 (2001).
- [11] T. Muta, A. Sugamoto, M. Z. Yang, and Y. D. Yang, Phys. Rev. D **62**, 094020 (2000);
- [12] M. Z. Yang and Y. D. Yang, Phys. Rev. D **62**, 114019 (2000);
- [13] D. s. Du, D. s. Yang, and G. h. Zhu, Phys. Rev. D **64**, 014036 (2001); Phys. Lett. B **509**, 263 (2001); **488**, 46 (2000);
- [14] H. Y. Cheng and K. C. Yang, Phys. Lett. B **511**, 40 (2001); Phys. Rev. D **64**, 074004 (2001); **63**, 074011 (2001).
- [15] D. s. Du, H. u. Gong, J. f. Sun, D. s. Yang, and G. h. Zhu, Phys. Rev. D **65**, 074001 (2002);
- [16] D. s. Du, H. j. Gong, J. f. Sun, D. s. Yang, and G. h. Zhu, Phys. Rev. D **65**, 094025 (2002); **66**, 079904 (E) (2002).

- [17] D. s. Du, J. f. Sun, D. s. Yang, and G. h. Zhu, Phys. Rev. D **67**, 014023 (2003).
- [18] J. f. Sun, G. h. Zhu, and D. s. Du, Phys. Rev. D **68**, 054003 (2003).
- [19] M. Beneke, G. Buchalla, M. Neubert, and C. T. Sachrajda, Nucl. Phys. B **675**, 333 (2003).
- [20] X. Q. Li, G. r. Lu, and Y. D. Yang, Phys. Rev. D **68**, 114015 (2003); **71**, 019902 (E) (2005);
- [21] X. q. Li and Y. d. Yang, Phys. Rev. D **72**, 074007 (2005).
- [22] D. s. Du, arXiv: hep-ph/0508287; M. Beneke, arXiv: hep-ph/0509297.
- [23] W. S. Hou, Nucl. Phys. B **308**, 561(1988).
- [24] J.-M. Gérard and W. S. Hou, Phys. Rev. Lett. **62**, 855 (1989); Phys. Rev. D **43**, 2909 (1991); Phys. Lett. B **253**, 478 (1991).
- [25] H. Simma and D. Wyler, Nucl. Phys. B **344**, 283 (1990); J. Liu and Y. P. Yao, Phys. Rev. D **41**, 2147 (1990).
- [26] C. Greub and P. Liniger, Phys. Rev. D **63**, 054025 (2001).
- [27] S. W. Bosch and G. Buchalla, Nucl. Phys. B **621**, 459 (2002); M. Beneke, T. Feldmann, and D. Seidel, Nucl. Phys. B **612**, 25 (2001); A. Ali and A. Y. Parkhomenko, Eur. Phys. J. C **23**, 89 (2002).
- [28] G. Eilam and Y. D. Yang, Phys. Rev. D **66**, 074010 (2002).
- [29] S. Mishima and A. I. Sanda, Prog. Theor. Phys. **110**, 549 (2003).
- [30] N. Cabibbo, Phys. Rev. Lett. **10**, 531 (1963); M. Kobayashi and T. Maskawa, Prog. Theor. Phys. **49**, 652 (1973).
- [31] A. Ali, G. Kramer, and C. D. Lu, Phys. Rev. D **58**, 094009 (1998); **59**, 014005 (1999).
- [32] Y. H. Chen, H. Y. Cheng, B. Tseng, and K. C. Yang, Phys. Rev. D **60**, 094014 (1999); **62**, 054029 (2000).

- [33] N. G. Deshpande, B. Dutta, and S. Oh, Phys. Lett. B **473**, 141 (2000).
- [34] A. S. Dighe, M. Gronau, and J. L. Rosner, Phys. Rev. D **57**, 1783 (1998); M. Gronau, Phys. Rev. D **62**, 014031 (2000); M. Gronau and J. L. Rosner, Phys. Rev. D **61**, 073008 (2000).
- [35] R. Aleksan, P. F. Giraud, V. Morenas, O. Pene, and A. S. Safir, Phys. Rev. D **67**, 094019 (2003).
- [36] G. Buchalla, A. J. Buras, and M. E. Lautenbacher, Rev. Mod. Phys. **68**, 1125 (1996).
- [37] A. J. Buras, arXiv:hep-ph/9806471; Lect. Notes Phys. **558**, 65 (2000);
- [38] C. D. Lü, K. Ukai, and M. Z. Yang, Phys. Rev. D **63**, 074009 (2001).
- [39] A. Kagan, Phys. Lett. B **601**, 151 (2004).
- [40] T. Feldmann and T. Hurth, J. High Energy Phys. **11**, 037 (2004).
- [41] N. de. Groot, W. N. Cottingham, I. B. Whittingham, Phys. Rev. D **68**, 113005 (2003).
- [42] S. Mishima and A. I. Sanda, Prog. Theor. Phys. **110**, 549 (2003).
- [43] Heavy Flavour Averaging Group, <http://www.slac.stanford.edu/xorg/hfag>.
- [44] A. J. Buras, R. Fleischer, S. Recksiegel, and F. Schwab, Phys. Rev. Lett. **92**, 101804 (2004); Nucl. Phys. B **697**, 133 (2004).
- [45] W. M. Sun, Phys. Lett. B **573**, 115 (2003); C. W. Chiang, arXiv: hep-ph/0502183.
- [46] R. Fleischer and T. Mannel, Phys. Rev. D **57**, 2752 (1998); A. J. Buras and R. Fleischer, Eur. Phys. J. C **11**, 93 (1999); **16**, 97 (2000).
- [47] M. Beneke and S. Jager, arXiv: hep-ph/0512351.
- [48] A. J. Buras, P. Gambino, U. A. Haisch, Nucl. Phys. B **570**, 117 (2000).
- [49] L. Wolfenstein, Phys. Rev. Lett. **51**, 1945 (1983).
- [50] S. Eidelman, *et al.*, Phys. Lett. B **592**, 1 (2004).

- [51] M. Beneke and T. Feldmann, Nucl. Phys. **B592**, 3 (2001); M. Beneke, Nucl. Phys. Proc. Suppl. **111**, 62 (2002).
- [52] A. G. Grozin and M. Neubert, Phys. Rev. D **55**, 272 (1997).
- [53] B. V. Geshkenbein and M. V. Terentev, Yad. Fiz. **40**, 758 (1984) [Sov. J. Nucl. Phys. **40**, 487 (1984)].
- [54] P. Ball and V. M. Braun, Phys. Rev. D **58**, 094016 (1998); P. Ball, J. High Energy Phys. **09**, (1998) 005.
- [55] V. M. Braun and I. E. Filyanov, Z. Phys. C **48**, 239 (1990).
- [56] T. Feldmann and T. Hurth, J. High Energy Phys. **11**, (2004) 037.
- [57] V. M. Braun, D. Y. Ivanov, and G. P. Korckemsky, Phys. Rev. D **69**, 034014 (2004).
- [58] A. Khodjamirian, T. Mannel, and N. Offen, Phys. Lett. B **620**, 52 (2005).
- [59] A. Gray *et al.* [HPQCD Collaboration], Phys. Rev. Lett. **95**, 212001 (2005)
- [60] P. Ball and R. Zwicky, Phys. Rev. D **71**, 014015 (2005); Phys. Rev. D **71**, 014029 (2005); Phys. Lett. B **633**, 289 (2006);
- [61] L-n, Li, S. Mishima and A.I. Sanda, Phy. Rev. **D72**, 114005(2005); L-n, Li, S. Mishima, hep-ph/0602214.